RSC Advances

PAPER

View Article Online
View Journal | View Issue

Cite this: *RSC Adv.*, 2023, **13**, 12589

A new class of anti-proliferative activity and apoptotic inducer with molecular docking studies for a novel of 1,3-dithiolo[4,5-*b*]quinoxaline derivatives hybrid with a sulfonamide moiety†

Mostafa A. Ismail,[a] Moustafa S. Abusaif,[b] Mohamed S. A. El-Gaby,*[b] Yousry A. Ammar*[b] and Ahmed Ragab*[b]

A new series of 6-(pyrrolidin-1-ylsulfonyl)-[1,3]dithiolo[4,5-*b*]quinoxaline-2-ylidines **10a–f**, **12**, **14**, **16**, and **18** were designed, synthesized, and evaluated for their *in vitro* anticancer activity. The structures of the novel compounds were systematically characterized by ^{1}H NMR, ^{13}C NMR, and elemental analysis. The synthesized derivatives were evaluated for their *in vitro* antiproliferative activity against three human cancer cell lines (HepG-2, HCT-116, and MCF-7) with more sensitivity to MCF-7. Moreover, three derivatives **10c**, **10f**, and **12** were the most promising candidates with sub-micromole values. These derivatives were further evaluated against MDA-MB-231, and the results displayed significant IC_{50} values ranging from 2.26 ± 0.1 to 10.46 ± 0.8 μM and showed low cellular cytotoxicity against WI-38. Surprisingly, the most active derivative **12** revealed sensitivity towards the breast cell lines MCF-7 (IC_{50} = 3.82 ± 0.2 μM) and MDA-MB-231 (IC_{50} = 2.26 ± 0.1 μM) compared with doxorubicin (IC_{50} = 4.17 ± 0.2 and 3.18 ± 0.1 M). Cell cycle analysis showed that compound **12** arrests and inhibits the growth of MCF-7 cells in the S phase with values of 48.16% compared with the untreated control 29.79% and exhibited a significantly higher apoptotic effect in MCF-7 with a value of 42.08% compared to control cell at 1.84%. Furthermore, compound **12** decreased Bcl-2 protein 0.368-fold and activation on pro-apoptotic genes Bax and P53 by 3.97 and 4.97 folds, respectively, in MCF-7 cells. Compound **12** exhibited higher inhibitory activity to $EGFR^{Wt}$, $EGFR^{L858R}$, and VEGFR-2 with IC_{50} values (0.19 ± 0.009, 0.026 ± 0.001, and 0.42 ± 0.021 μM) compared with erlotinib (IC_{50} = 0.037 ± 0.002 and 0.026 ± 0.001 μM) and sorafenib (IC_{50} = 0.035 ± 0.002 μM). Finally, *in silico* ADMET prediction presented that 1,3-dithiolo[4,5-*b*]quinoxaline derivative **12** obeys the Lipinski rule of five and the Veber rule with no PAINs alarms and moderately soluble properties. Additionally, toxicity prediction revealed that compound **12** demonstrated inactivity to hepatotoxic carcinogenicity, immunotoxicity, mutagenicity, and cytotoxicity. Moreover, molecular docking studies showed good binding affinity with lower binding energy inside the active site of Bcl-2 (PDB: 4AQ3), EGFR (PDB: 1M17), and VEGFR (PDB: 4ASD).

Received 13th March 2023
Accepted 10th April 2023

DOI: 10.1039/d3ra01635h

rsc.li/rsc-advances

1. Introduction

Cancer is a leading cause of death and a worldwide public health issue. Numerous potent anticancer medications are available, including classic chemotherapy drugs that prevent cell proliferation and DNA replication.[1] The greatest cause of mortality worldwide is cancer, which claims 1.61 million lives annually (19.41%) including 0.79 million from liver cancer (9.2%), and 0.79 million from stomach cancer (9.2%).[2,3] In addition, breast cancer is the most commonly diagnosed cancer in women, with 287 000 women expected to receive a diagnosis by 2022.[4] Despite early detection and treatment advances, patients with distant metastases of breast cancer often get poor results due to their low incomes and the high cost of therapies.[5] Most breast cancer-related deaths result from metastasis to distant organs,[6] highlighting the need to find pathways or cell populations that promote and accelerate breast cancer metastasis. In breast tumors, a small percentage of cells, known as breast cancer stem cells (BCSCs), are still capable of self-renewing and regenerating the heterogeneous tumor lesions, which is referred to as tumor recurrence.[7,8] These BCSCs are rare, often quiescent, highly ATP-binding cassette transporter-expressed, maintain an increased DNA-repair capability, and resist high concentrations of reactive oxygen species (ROS),

[a]*Chemistry Department, Faculty of Science, Al-Azhar University, Assiut, 71524, Egypt*
[b]*Chemistry Department, Faculty of Science (Boys), Al-Azhar University, Nasr City, Cairo, 11884, Egypt. E-mail: m_elgaby@azhar.edu.eg; yossry@azhar.edu.eg; Ahmed_ragab@azhar.edu.eg; Ahmed_ragab7@ymail.com*

† Electronic supplementary information (ESI) available. See DOI: https://doi.org/10.1039/d3ra01635h

contributing to therapeutic resistance and poor patient prognoses.[4] The clinical need to research and therapeutically target these cell types is supported by the fact that BCSCs cause metastasis and contribute to therapy resistance.[9] One of the most important signaling proteins regulating the tumor angiogenesis process is the vascular endothelial growth factor (VEGF).[10] VEGF overexpression was found in several cancers, including breast carcinoma.[11,12] Tyrosine kinase receptors VEGFR-1, VEGFR-2, and VEGFR-3 are involved in the angiogenic process through their interactions with VEGF ligands. VEGFR-2 mediates all VEGF responses in endothelial cells.[13,14] Therefore, developing effective medications for human angiogenesis-dependent cancers should focus on targeting VEGFR-2.[15] The FDA has licensed a number of VEGFR-2 suppressors for treating different malignancies.[16,17] In general, VEGFR-2 kinase inhibitors are divided into two major categories. Type I kinase inhibitors compete with ATP for ATP-binding sites (ATP competitive inhibitors). In contrast, the second type induces the DFG-out (inactive) conformation of the enzyme to enter an allosteric region (near ATP binding site), which is only visible in the inactive DFG-out conformation.[18–20] However, several downsides, such as bleeding complications, have been noted during clinical use; as a result, there is still an urgent need to develop safe VEGFR-2 inhibitors.[21]

Furthermore, the epidermal growth factor receptor (EGFR) is an attractive therapeutic target for cancer treatment due to its association with the regulation of cell survival, proliferation, metastasis, and angiogenesis, as well as its widespread

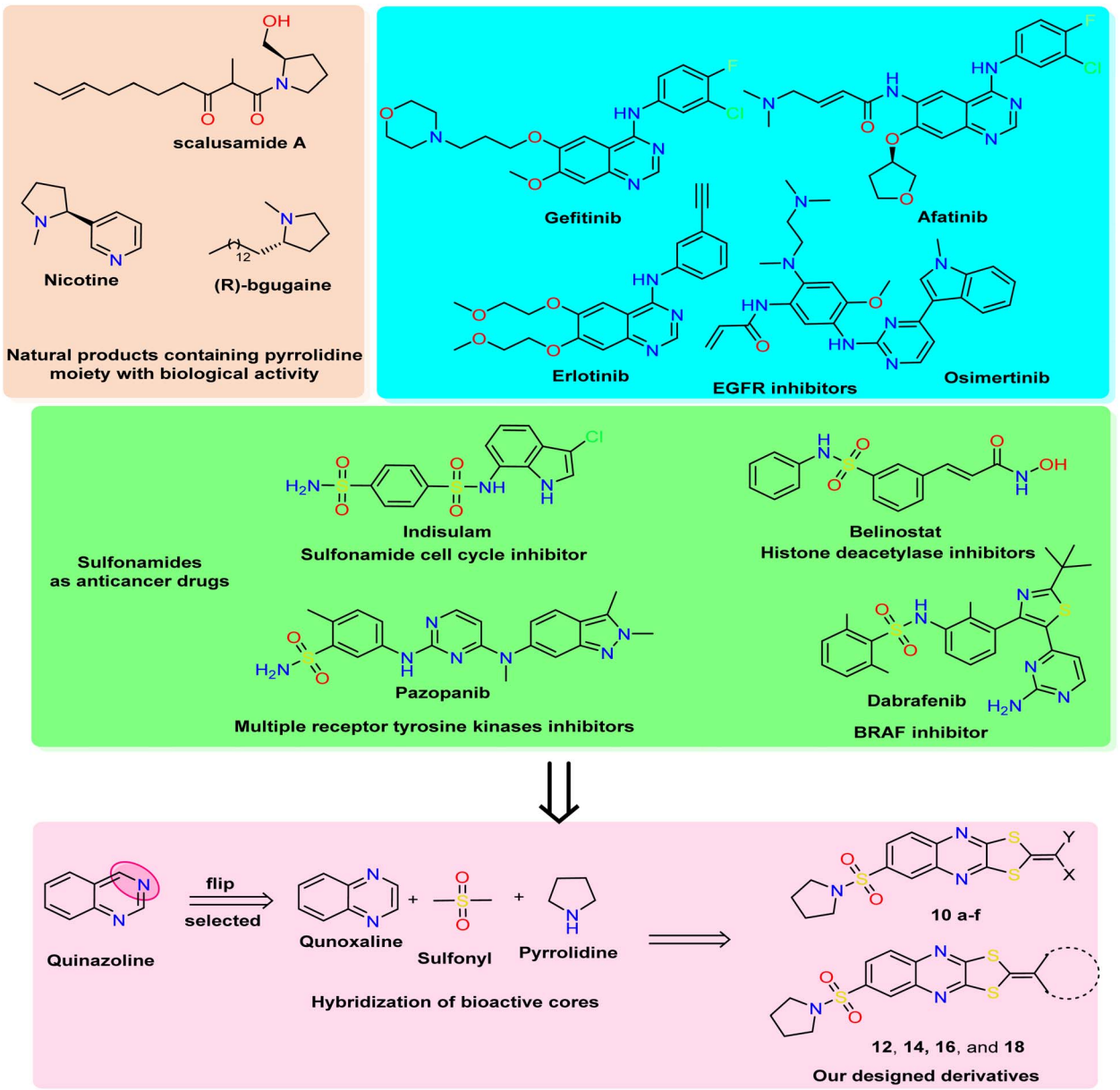

Fig. 1 Rational study involved the most bioactive cores as quinazoline (quinoxaline analog), pyrrolidine, and sulfonamide moiety, and our newly designed 1,3-dithiolo[4,5-*b*]quinoxaline derivatives.

overexpression in a wide range of solid tumors.[22] Since the first-generation EGFR-TKI, gefitinib, was introduced in 2002 (Japan), EGFR-TKIs have evolved into three generations, involving more than a dozen medications.[23] EGFR-TKIs have evolved into three generations in the past two decades, involving more than a dozen medications since the first-generation EGFR-tyrosine kinase inhibitor (TKI), Gefitinib, was introduced in 2002 (Japan). The first generation of EGFR-TKIs, which includes Gefitinib and erlotinib, inhibits the binding of ATP to the TK domain.[24,25] Despite the effectiveness of the first therapy, after 9–14 months of clinical therapy, patients developed acquired drug resistance, and at least 50% of them had the T790M mutation.[26] The second generation of inhibitors, which were released in 2013 to combat drug resistance, interacted with Michael receptors and the sulfhydryl groups of Cys in mutant kinase to create covalent binding complexes such as afatinib, which has substantial negative effects in the clinic and is infrequently utilized due to its poor selectivity for mutant *versus* wild-type EGFR[27] (Fig. 1). Moreover, the third generation was approved by the FDA in November 2015 to treat non-small-cell lung cancer (NSCLC) patients who were using EGFR kinase inhibitors and had a metastatic EGFR T790M mutation as osimertinib and olmutinib. Osimertinib received additional FDA approval in April 2018 as a first-line treatment for people with metastatic NSCLC who had EGFR mutations (EGFR 19Del or EGFR L858R).[28–30] These substances exhibit specific toxicity toward the tumor endothelial cells needed for the malignancy formation and significant cytotoxicity against a wide range of human cancer cell lines. They thus represent a novel family of vascular disrupting medicines that significantly shut off the blood supply to tumors, resulting in the necrosis and apoptosis of cancer cells.[31–33]

In medicinal chemistry, quinoxalines and quinoxalinones are desirable chemical candidates and are considered analogies for quinazoline by flipping carbon–nitrogen atoms at positions three and four. The quinoxaline derivatives exhibited a variety of biological targets due to their ability to cause biological reactions with biological targets. They, therefore, displayed antiviral,[34] herbicidal,[35] antimicrobial,[36] anticancer,[37] and anti-inflammatory[38] effects. Additionally, several antibiotics, such as echinomycin, levomycin, and actinoleutin, have a quinoxaline moiety in their structures and are known to impede the development of Gram-positive bacteria.[39,40] The quinoxaline scaffold also provides the foundation for many essential aspects in addition to these medical applications. The pharmacological potential of quinoxalines as anticancer drugs has just come to light,[41,42] and several theoretical research on quinoxaline and its derivatives have been carried out to discover new antineoplastic molecules. Porter and collaborators' research recently identified the quinoxaline scaffold as a template for creating c-Met kinase inhibitors.[43]

The polythia-heterocyclic molecules are uncommon and interesting heterocyclic classes that exhibited a wide range of biological activities, especially 1,2-dithiole and 1,3-dithiole.[44,45] The 1,2-dithiole derivatives have been isolated from cruciferous vegetables and are protective phytochemicals.[46,47] Moreover, 1,3-dithiol-2-ylidenes is a building block for electronic materials.[48] The importance of 1,2-dithiol and 1,3-dithiol-2-ylidenes is related to their ability to donate electrons.[49] Additionally, it was reported that 2-ylidene-1,3-dithiolane derivatives revealed a variety of biological activities as antimicrobial,[50] insecticidal,[51] and anticancer activities.[52] For drug design and pharmaceutical industries, a pyrrolidine scaffold is a preferred scaffold[53] and is ranked within the top five common five-membered nitrogen heterocyclic compounds. Additionally, the pyrrolidine moiety was approved by nearly 37 FDA drugs in the United States.[54] Pyrrolidines have various pharmacological activities, including cholinesterase inhibitory,[55] anti-HIV,[56] antimicrobial,[57] anti-inflammatory,[58] antioxidant,[59] and anticancer properties.[60] In natural products with saturated ring systems, the pyrrolidine moiety is typically found in plants or microbially derived alkaloids[61] that exhibit a variety of bioactivities, including scalusamides A (antimicrobial activities), nicotine (have anti-inflammatory, antioxidant, and antihyperglycemic), and (*R*)-bgugaine (anticancer activity)[62] The sulfonamide moiety is a key component of numerous clinical drugs with broad-spectrum applications in medicine, pharmaceuticals, and pharmacology, such as antiviral, protease inhibitor, anti-inflammatory, anti-epileptic, anti-diabetic, anti-tumor, and antibacterial activities.[63] One aryl sulfonamide medication with anticancer efficacy is indisulam, which produced cell cycle arrest in the G1 phase and cell death[64] (Fig. 1). Indisulam's SAR study revealed that its sulfonamide group is crucial for its anticancer effects. More critically, the mitotic arrest phenotype is strongly influenced by the aryl group and substituent.[65] Many anticancer drugs containing sulfonamide moiety, such as pazopanib inhibit tumor growth and angiogenesis by targeting multiple receptor tyrosine kinases.[66] Additionally, belinostat is a histone deacetylase inhibitor used to treat cancers of the blood and solid tissues.[67] The drug dabrafenib is used in the treatment of certain types of cancer, including melanoma, non-small-cell lung cancer, and thyroid cancer (BRAF inhibitor)[68] (Fig. 1).

Based on all the above facts and in continuation of our work in the design and synthesis of new heterocyclic bioactive cores by hybridization approach for use in medicinal chemistry.[69–73] Our work involved synthesizing a new series of 1,3-dithiolo[4,5-*b*]quinoxaline derivatives tagged with pyrrolidinosulfonyl moiety in one bioactive scaffold. Additionally, the designed derivatives were evaluated as antiproliferative activity against three human cancer cell lines (HepG2, HCT-116, and MCF-7) using the MTT assay. Moreover, the most active derivatives were screened for other breast cancer cells (MDA-MB-231) using a non-tumorigenic normal cell line (WI-38). Besides, the most active member was selected to determine the effect on apoptosis detection studies, including cell-cycle and apoptosis analysis, mitochondrial apoptosis pathway proteins (BAX, Bcl-2, and p53), and tyrosine kinases enzymes (EGFR and VEGFR). Finally, the *in silico* ADMET and docking simulation were determined and discussed.

2. Results and discussion

2.1. Chemistry

The designed target compounds 1,3-dithiolo[4,5-*b*]quinoxalin-2-ylidenes **10a–f**, **12**, **14**, **16**, and **18** are depicted in (Schemes

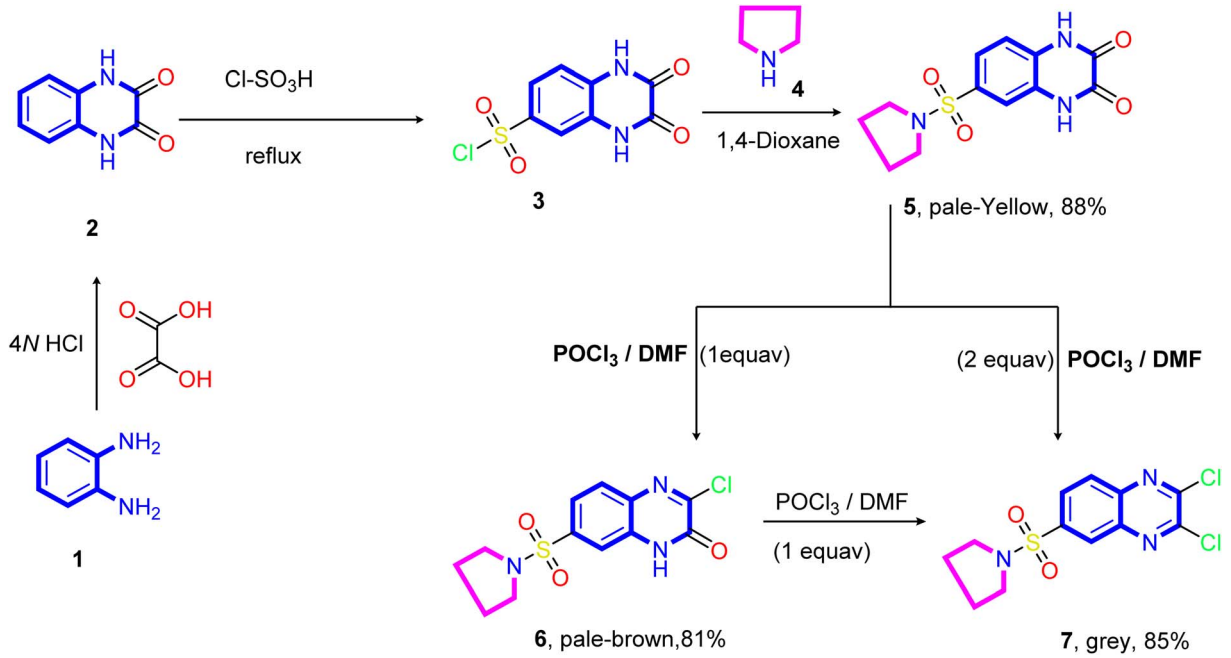

Scheme 1 Synthetic pathways of the 2,3-dioxo-1,2,3,4-tetrahydroquinoxaline-6-sulfonyl chloride **3**, 3-chloro-6-(pyrrolidin-1-ylsulfonyl)quinoxalin-2(1*H*)-one **6**, and 2,3-dichloro-6-(pyrrolidin-1-ylsulfonyl)quinoxaline **7**.

2–4). The key intermediate 2,3-dioxo-1,2,3,4-tetrahydroquinoxaline-6-sulfonyl chloride **3** was obtained by condensing *o*-phenylenediamine **1** with oxalic acid in the presence of aqueous hydrochloric acid to form 1,4-dihydroquinoxaline-2,3-dione **2**, which was subsequently treated with chlorosulfonic acid according to the previously reported procedure[74–76] (Scheme 1).

Treatment of sulfonyl chloride derivative **3** with pyrrolidine **4** in refluxing 1,4-dioxane afforded the corresponding 6-(pyrrolidin-1-ylsulfonyl)-1,4-dihydro quinoxaline-2,3-dione **5** in good yield (88%). The structure of compound **5** was established on the basis of its elemental analysis and spectral data. Its infrared spectrum showed characteristic absorption band at ν 3502 and 3366 cm^{-1} for the NH stretching, 1692 cm^{-1} for the two carbonyl groups (C=O stretching), 1613 cm^{-1} for the C=N stretching, and (ν 1330 and 1148 cm^{-1}) for the SO_2 stretching vibrations. Moreover, the quinoxalinedione intermediate **5** was subjected to react with an equimolar amount of phosphorus oxychloride in *N*,*N*-dimethylformamide, and 3-chloro-6-(pyrrolidin-1-ylsulfonyl)quinoxalin-2(1*H*)-one **6** was obtained. The structure of compound **5** was confirmed on the basis of microanalysis and spectral data. The infrared spectrum of compound **5** indicated characteristic absorption bands at ν 3401 cm^{-1} and 1694 cm^{-1} due to NH and carbonyl stretching vibrations, respectively. The band observed at 1555 cm^{-1} is due to C=N stretching vibration of the quinoxaline pharmacophore. On the other hand, refluxing of quinoxalinedione **5** with two equivalents of phosphorus oxychloride in *N*,*N*-dimethylformamide afforded the 2,3-dichloro-6-(pyrrolidin-1-ylsulfonyl) quinoxaline **7**.

Further, the structure of compound **7** was confirmed on the basis of its elemental analysis, spectral data, and an independent synthesis by reacting an equimolar amount of phosphorus oxychloride in *N*,*N*-dimethylformamide under reflux. The infrared spectrum of compound **7** indicated the absence of the carbonyl absorption band and the presence of the characteristic absorption band at ν 1615 cm^{-1} for the C=N group. Its ^{1}H NMR spectrum (DMSO-d_6) revealed a quintet at δ 1.63 ppm for the methylene protons at 3- and 4-positions of the pyrrolidine ring and a triplet at δ 3.26 ppm, which are readily assigned to (CH_2–N–CH_2) protons present in the pyrrolidine ring. The two doublets at δ 8.22 and 8.28 ppm with coupling constant (J = 8.0 Hz) assigned to the hydrogen attached at C_5 and C_6 of the quinoxaline ring, and a sharp singlet at δ 8.42 assigned to the hydrogen at C_8 of the quinoxaline ring. Moreover, the ^{13}C NMR spectrum showed the presence of two signals at δ 25.10 and 48.31 assigned to two methylene groups at C_3, C_4, and two CH_2 at (C_2 and C_4) of the pyrrolidine ring, respectively. In addition, six signals at δ 125.99, 127.68, 130.03, 138.99, 139.53, and 141.78 ppm (C–SO_2) equivalent to the C_6H_3 group, and two downfield signals at δ 147.09 and 147.77 ppm for the two C=N are attached to the chlorine atom.

Our approach to annulate the 1,3-dithiol-2-ylidene group to the quinoxaline ring was based on the good nucleophilicity of the potassium ethene-1,1-dithiolates anion and the fact that the nucleophilic aromatic substitution reactions are known to occur on 2,3-dichloroquinoxaline core.[77] Initially, potassium ethene-1,1-bis-(thiolates) **9** are prepared by reacting an acyclic active methylene compound **8** with carbon disulfide in the presence of two equivalents of the base at room temperature. As viewed in Scheme 2, the treatment of 2,3-dichloro-6-(pyrrolidin-1-ylsulfonyl) quinoxaline **7** with potassium ethene-1,1-bis-(thiolates) **9** at room temperature in *N*,*N*-dimethylformamide

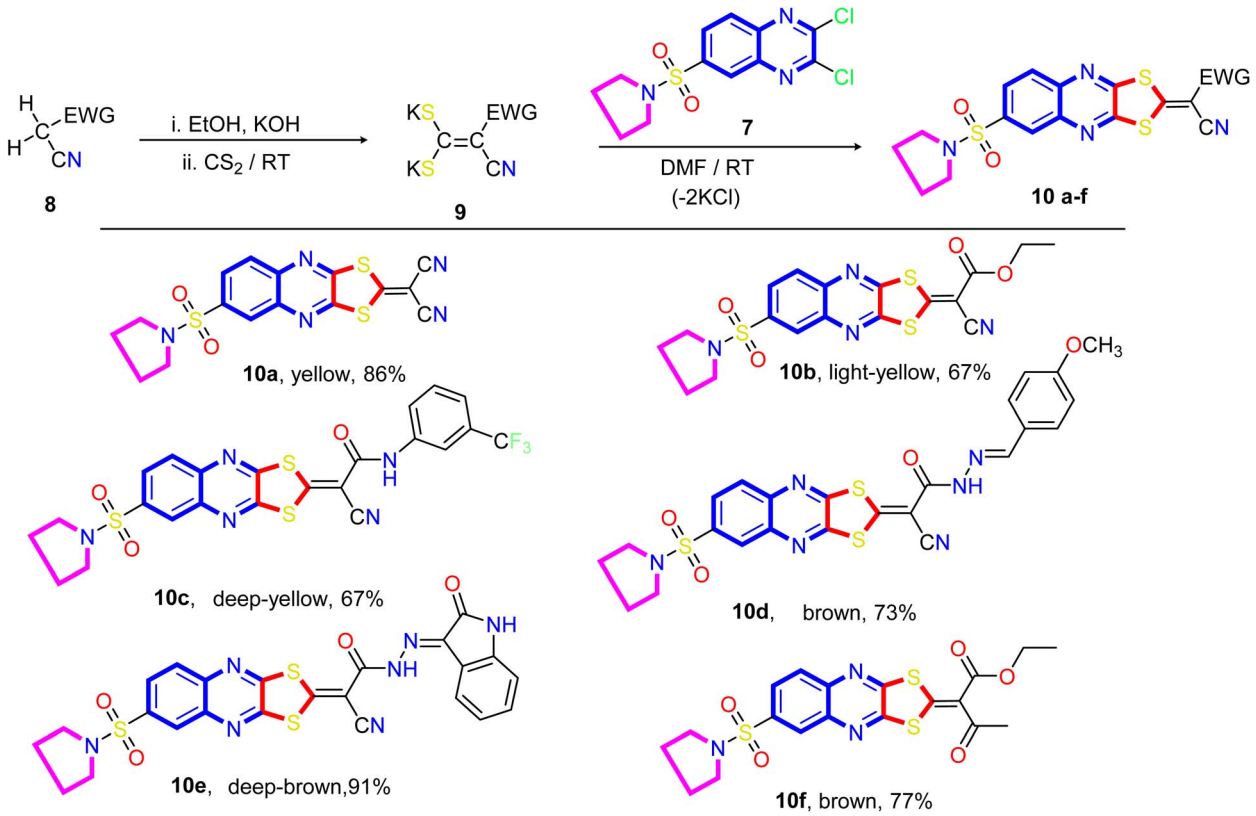

Scheme 2 Synthetic pathways of the target 6-(pyrrolidin-1-ylsulfonyl)-[1,3]dithiolo[4,5-*b*]quinoxaline-2-ylidines (**10a–f**).

afforded the novel 2-ylidene-6-(pyrrolidin-1-ylsulfonyl)-[1,3] dithiolo[4,5-*b*]quinoxalines **10a–f** in good yields. The structure of the reaction products is established on the basis of their elemental analysis and spectral data. The infrared spectra of compounds **10a–f** showed the characteristic absorption bands for the -ylidene group (C=C). The IR spectrum of compound **10a** taken as a representative example of the series, showed three absorption bands at ν 2219, 2193, and 1621 cm^{-1} due to two cyano and C=N, respectively, besides absorption bands at ν 1550 cm^{-1} assignable for the C=C group. The representative ^1H

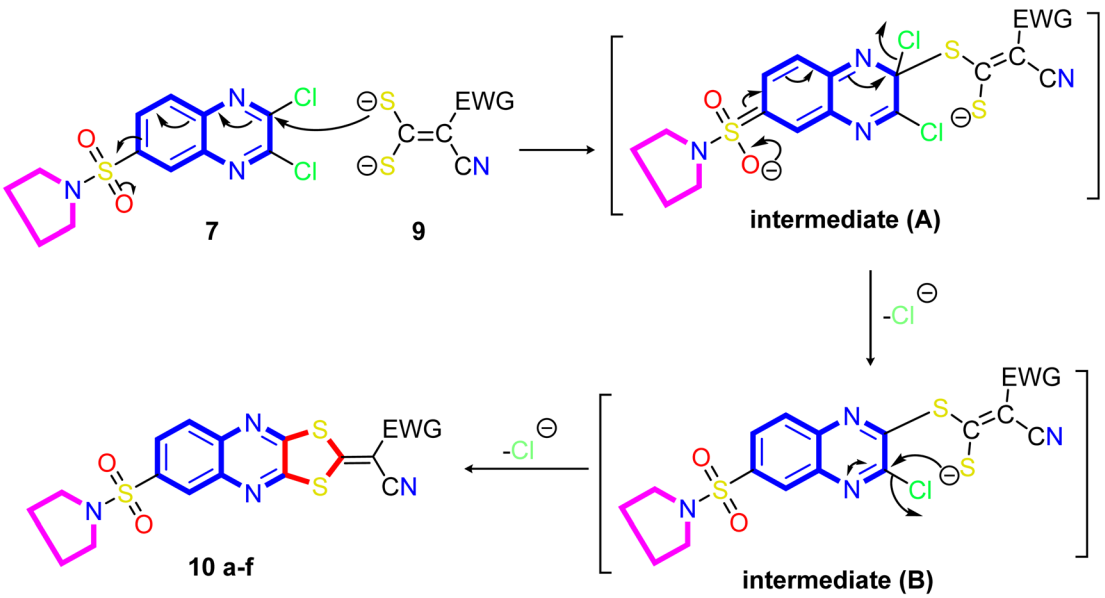

Scheme 3 Illustration on the resection mechanism of bi-nucleophile 1,3-dithiolo with unsymmetrical from bi-electrophile and 2,3-dichloro derivative 7.

NMR spectrum of compound **10b** (DMSO-d_6) revealed a triplet at δ 1.33 ppm, a quartet at δ 4.37 ppm assigned to the ethyl group, a quintet at δ 1.33 ppm assigned to the methylene protons at 3- and 4-positions of the pyrrolidine ring, and a triplet signal at δ 3.27 ppm, which was readily assigned to CH_2–N–CH_2 protons present in the pyrrolidine ring. The signals appeared at δ 8.15 ppm (d, 1H, J = 8.0 Hz), at δ 8.29 ppm (d,1H, J = 8.0 Hz), and a sharp singlet at δ 8.29 ppm can be assigned to C_7, C_8, and C_5 of the quinoxaline ring, respectively. The ^{13}C NMR spectrum revealed signals at δ 14.02 for methyl, signals at δ 24.94 and 48.17 ppm for four methylene groups of the pyrrolidine motif, a signal at δ 62.72 ppm for OCH_2 of the ethoxy group, two signals at δ 92.39 and 114.45 for the two cyano groups (CN), and signals at δ 122.33, 125.06, 126.40, 136.68, 137.17, 138.16, 149.95, and 151.26 ppm are assigned to the corresponding different types of carbon atoms present in the compound. The most downfield signals appeared at δ 167.57 and 165.86 ppm, which could be assigned to the carbonyl and ethylenic groups.

A proposed mechanism for forming 2-ylidene-[1,3]dithiolo [4,5-*b*]quinoxalines **10a–f** is described in Scheme 3. The formation of [1,3]dithiolo[4,5-*b*]quinoxalines **10a–f** are assumed to proceed *via* nucleophilic addition of ethene-1,1-dithiolates anion **9** to the activated double bond at position-3 in 2,3-dichloro-6-(pyrrolidin-1-ylsulfonyl)quinoxaline **7** to give the non-isolable intermediate **A** and **B**, followed by intramolecular cyclization by elimination of potassium chloride to afford the final product **10**, Scheme 3. The structures of [1,3]dithiolo[4,5-*b*] quinoxalines **10a–f** have been further confirmed from independent work *via* a one-pot, three-component, reaction of active methylene compounds with carbon disulfide in the presence of a base, followed by *in situ* coupling of the resulting dithioate salts with 2,3-dichloro-6-(pyrrolidin-1-ylsulfonyl) quinoxaline **7** to afford a product identical in all respect (m.p., mixed M.p., TLC, and spectra).

Our study was extended to include synthesizing novel [1,3] dithiolo[4,5-*b*]quinoxaline linked to cyclohexyl, pyrazolyl, and pyrimidinyl moieties. Thus, the reaction of the dithioate salts derived from cyclic active methylene compounds **11**, **13**, **15**, and **17** with compound **7** in *N*,*N*-dimethylformamide at room temperature gave the corresponding [1,3]dithiolo[4,5-*b*]quinoxalines **12**, **14**, **16** and **18**, respectively (Scheme 4).

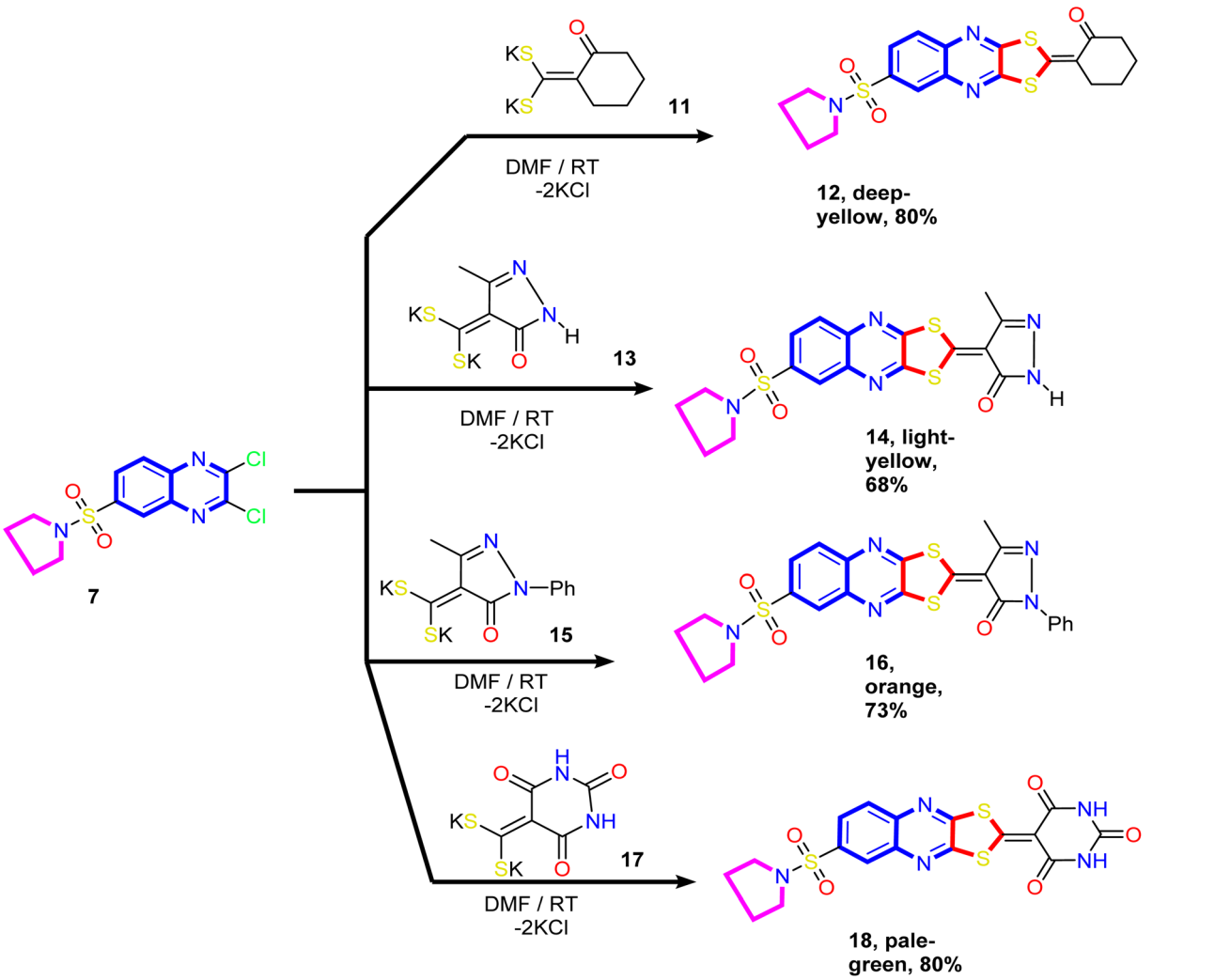

Scheme 4 Synthesis of novel [1,3]dithiolo[4,5-*b*]quinoxalines **12**, **14**, **16**, and **18** linked to cyclohexyl, pyrazolyl, and pyrimidinyl moieties.

The analytical and spectral data of compounds **12**, **14**, **16**, and **18** were in agreement with their proposed structure. Thus, the ^{1}H NMR spectrum of compound **14** showed a quintet at δ 1.69 ppm assigned to methylene protons (C_3 and C_4) of the pyrrolidine ring, a triplet at δ 3.27 ppm assigned to methylene protons (C_2 and C_5) of the pyrrolidine ring, and a singlet at δ 2.39 ppm assigned to methyl protons at position-4 of the pyrazole ring. The two doublets at δ 8.19 ppm and 8.27 ppm and a sharp singlet at δ 8.30 ppm were readily assigned to the hydrogen attached at C_5, C_6, and C_8 of the quinoxaline ring, respectively. The downfield singlet signal at δ 11.58 ppm corresponds to the pyrazole ring's NH. In addition, the ^{13}C NMR spectrum revealed signals at δ 14.54 (CH_3), 25.74 ($2CH_2$; pyrrolidine), 50.61 ($2CH_2$; pyrrolidine), and signals at δ 103.72, 128.34, 130.73, 132.22, 136.37, 137.46, 140.62, 145.02, 149.27, and 152.61 ppm corresponding to a different type of carbon atoms present in the compound. The most downfield signal appeared at δ 177.76 and 169.17 ppm attributed to the C=O and C=C groups, respectively.

2.2. Biological activity

2.2.1. *In vitro* cytotoxicity screening and structure–activity relationship (SAR) study. The newly designed 6-(pyrrolidin-1-ylsulfonyl)quinoxaline derivatives **7**, **10**, **12**, **14**, **16**, and **18** were assessed for their *in vitro* antiproliferative activity against three human cancer cell lines (HepG2, HCT-116, and MCF-7) using MTT assay as described previously,[37,78] while maintaining doxorubicin as a standard drug. The half-maximal inhibitory concentration (IC_{50}) of the synthesized derivative was measured and expressed in μM. As represented in Table 1, the tested derivatives exhibited good to moderate potency, with three derivatives **10c**, **10f**, and **12** that exhibited the most promising candidates against the tested strains. Additionally, all tested compounds inhibited the cancer cells in a dose-dependent manner. Based on the structure–activity relationship, our work was designed to study the activity of different fragments attached to position two in 1,3-dithiolo[4,5-*b*]quinoxaline derivative by two series, acyclic compounds **10a–f** and cyclic derivative **12–18**. Generally, the tested derivatives exhibited activity in the breast cancer cell line (MCF-7) rather than the colon cell line (HCT-116) and liver cell line (HepG2).

Firstly, modification of 1,3-dithiolo[4,5-*b*]quinoxaline derivative with acyclic acetonitrile moiety displayed moderate activity, where the presence of cyan acetonitrile moiety as compound **10a** causes a decrease in the activity over all cell lines (IC_{50} ranging between 79.42 ± 4.1–93.76 ± 4.7 μM) and replacing one cyano group by ethyl ester group as compound **10b** does not enhance the activity (IC_{50} ranging from 74.49 ± 3.9 to 87.41 ± 4.2 μM). At the same time, introducing 2-cyanoacetohydrazone with an electron-withdrawing group (CF_3) at the phenyl group to 1,3-dithiolo[4,5-*b*]quinoxaline pharmacophore, as represented in compound **10c**, revealed antiproliferative activity with IC_{50} values ranging from 6.13 ± 0.4 to 17.01 ± 1.3 μM relative to doxorubicin (4.17 ± 0.2–5.23 ± 0.3 μM) against the tested cell lines and this activity might be related to the presence of *N*-(3-trifloromethylphenyl) group. Moreover, combining the 1,3-dithiolo[4,5-*b*]quinoxaline derivative with 2-cyanoacetohydrazones with different fragments in hydrazone as compounds **10d** and **10e** exhibited good to moderate activity with IC_{50} ranging from 11.29 ± 0.9 to 41.90 ± 2.5 μM. In addition, the 2-cyanoacetohydrazone derivative **10d** that involved 4-methoxybenzylidene core revealed antiproliferative activity with IC_{50} values ranging from 11.29 ± 0.9 to 32.12 ± 2.2 μM better than 2-oxoindolin-3-ylidene derivative **10e** (IC_{50} range from 22.02 ± 1.7 to 41.90 ± 2.5 μM). Meanwhile, compound **10f** demonstrated good antiproliferative activity against (HepG2 = 26.77 ± 1.9 μM and HCT-116 = 12.51 ± 1.0 μM). Besides, compound **10f** showed promising activity against MCF-7 with an IC_{50} value of 8.78 ± 0.6 μM relative to doxorubicin (IC_{50} = 4.17 ± 0.2 μM).

For the second series that appears in Scheme 4, incorporating the 2-oxo-cyclohexan-2-ylidene to 1,3-dithiolo[4,5-*b*]quinoxaline derivative as compound **12** was revealed to be the most

Table 1 The *in vitro* cytotoxicity activity of the newly designed 6-(pyrrolidin-1-ylsulfonyl)-quinoxaline derivatives **7–18**[a]

	In vitro cytotoxicity activity represented by IC_{50} (μM)[b] ± SD/(SI)[c]				
	Cancer Cells				Normal cell
Cpd no	HepG2	HCT-116	MCF-7	MDA-MB-231	WI-38
7	48.74 ± 2.8	38.13 ± 2.2	31.04 ± 2.1	—	—
10a	89.72 ± 4.5	93.76 ± 4.7	79.42 ± 4.1	—	—
10b	80.30 ± 4.1	87.41 ± 4.2	74.49 ± 3.9	—	—
10c	**17.01 ± 1.3 (3.82)**	**9.26 ± 0.8 (7.01)**	6.13 ± 0.4 (10.61)	7.66 ± 0.5 (8.48)	65.06 ± 3.5
10d	32.12 ± 2.2	18.38 ± 1.4	11.29 ± 0.9	—	—
10e	41.90 ± 2.5	22.02 ± 1.7	24.30 ± 1.8	—	—
10f	**26.77 ± 1.9 (1.76)**	**12.51 ± 1.0 (3.69)**	8.78 ± 0.6 (5.27)	10.46 ± 0.8 (4.41)	46.18 ± 2.4
12	**8.25 ± 0.6 (9.89)**	**7.95 ± 0.5 (10.26)**	3.82 ± 0.2 (21.37)	2.26 ± 0.1 (36.12)	81.64 ± 4.1
14	68.97 ± 3.9	71.18 ± 3.8	70.11 ± 3.7	—	—
16	>100	>100	85.65 ± 4.3	—	—
18	83.38 ± 4.3	>100	62.84 ± 3.4	—	—
DOX	**4.50 ± 0.2**	**5.23 ± 0.3**	4.17 ± 0.2	3.18 ± 0.1	—

[a] (—) = not tested. [b] Averaging three independent results is used. [c] Selectivity index = (IC_{50} of WI-38)/(IC_{50} of cancer cell line).

potent candidate with IC_{50} values 8.25 ± 0.6, 7.95 ± 0.5, and 3.82 ± 0.2 μM compared with doxorubicin 4.50 ± 0.2, 5.23 ± 0.3, and 4.17 ± 0.2 μM against HepG2, HCT-116, and MCF-7, respectively. Moreover, replacing the cyclohexan-2-ylidene in compound **12** with heterocyclic cores as 1*H*-pyrazol-4-ylidene (compounds **14** and **16**) and pyrimidin-5-ylidene derivative (compound **18**) dramatically reduced the overall activity of the cell lines (IC_{50} = >68 μM), indicating that the antireflective activity preferred lipophilic group (CH_2) than hydrophilic atoms and groups (N and NH) in pyrazole and pyrimidine.

Moreover, the results found that the most active derivatives **10c**, **10f**, and **12** exhibited better cytotoxicity activity with IC_{50} values lower than the remaining compounds, especially against the MCF-7 ($IC_{50} \leq 8.78$ μM). Moreover, our work was extended to determine the most active three derivatives **10c**, **10f**, and **12**, against other breast cancer cells (MDA-MB-231) to confirm sensitivity against breast cancer. As described in Table 1, the results on these derivatives showed significant IC_{50} values ranging from 2.26 ± 0.1 to 10.46 ± 0.8 μM.

Furthermore, compound **12** was the most potent derivative with an IC_{50} value of 2.26 ± 0.1 μM followed by compound **10c** (IC_{50} = 7.66 ± 0.5 μM) and compound **10f** (IC_{50} = 10.46 ± 0.8 μM) relative to doxorubicin (IC_{50} = 3.18 ± 0.1 μM). Additionally, to determine the safety of these derivatives, the cytotoxic activity against non-tumorigenic normal cell line (WI-38) was investigated. The result displayed that these three derivatives **10c**, **10f**, and **12** showed low cellular cytotoxicity with IC_{50} values of 65.06 ± 3.5, 46.18 ± 2.4, and 81.64 ± 4.1 μM, respectively. Surprisingly, the selectivity index revealed that the highest value was observed by compound **12** against MDA-MB-231 with a value of 36.12, followed by MCF-7 (SI = 21.37) and confirmed selectivity and sensitivity to breast cancer.

Finally, for the screening study, it can be concluded that among the tested compounds, three derivatives **10c**, **10f**, and **12** showed promising activity against the tested cell line with safe cytotoxicity against WI-38. Moreover, compound **12** revealed the most active derivative and displayed sensitivity towards the breast cell lines MCF-7 and MDA-MB-231 with IC_{50} 3.82 ± 0.2 μM (1.09-fold increase) and 2.26 ± 0.1 μM (1.41-fold increase), as compared with doxorubicin (IC_{50} = 4.17 ± 0.2 and 3.18 ± 0.1 M), respectively.

2.2.2. Apoptosis detection studies

2.2.2.1 Cell cycle analysis and apoptosis induction by annexin-V assay. Antiproliferative agents often work by arresting the cell cycle at specific points, causing apoptosis.[79] The effect of the most potent 1,3-dithiolo[4,5-*b*]quinoxaline derivative **12** on the MCF-7 cell line at its IC_{50} value (3.82 μM) was studied, and a significant change was observed in the phases of the cell cycle, as described in Fig. 2. The target compound causes cell cycle arrest and inhibits the growth of MCF-7 cells in the S phase with values of 48.16% compared with untreated control at 29.79%. Meanwhile, a simultaneous decrease in the percentage of cells in the G0-G1 and G2/M phases with values of 48.16% and 7.32% compared with untreated breast cancer cells at 57.66 and 12.55%, respectively.

Furthermore, the ability of the most active derivative to induce apoptosis was confirmed by applying double staining of annexin-V/propidium iodide (PI) to stain DNA and, therefore, stated the dead cells. The most active derivative 1,3-dithiolo[4,5-*b*]quinoxaline derivative **12** exhibited a significantly higher apoptotic effect in MCF-7 with a value of 42.08% compared to that of control cell at 1.84%. Additionally, compound **12** displayed a remarkable increase in DNA content in early apoptosis with a value of 24.02 (54.59-folds) and late apoptosis with a value of 11.9 (79.33-folds) compared to the control, as described in Table 2 and Fig. 3.

2.2.2.2 Effect of the most active derivative compound 12 on mitochondrial apoptosis pathway proteins (BAX, Bcl-2, and p53). 2-(cyclohexan-2-ylidene)-[1,3]dithiolo[4,5-*b*]quinoxaline derivative **12**, which displayed the best cytotoxic activity on MCF-7 and MDA-MB-231, was further evaluated to some apoptosis marker, such as Bax and P53 (pro-apoptotic) and Bcl-2 (anti-apoptotic)

Table 2 Results of apoptosis and necrosis on MCF-7 of the most active 1,3-dithiolo[4,5-*b*]quinoxaline derivative **12**

	Apoptosis			
Cpd no.	Total	Early	Late	Necrosis
12/MCF-7	42.08	24.02	11.9	6.16
Cont.MCF-7	1.84	0.44	0.15	1.25

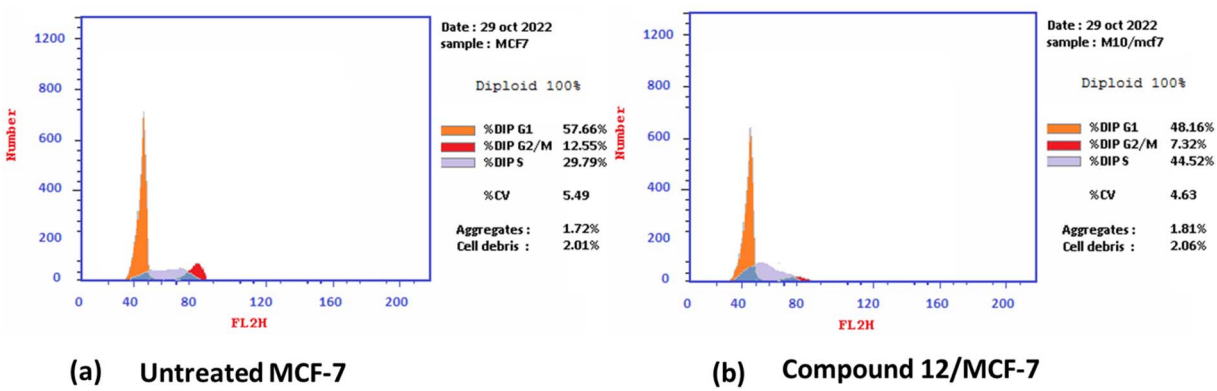

Fig. 2 Cell cycle distribution% assessment using FACS analysis (a) untreated cell; (b) compound **12** treated with MCF-7 at (IC_{50} = 3.82 μM).

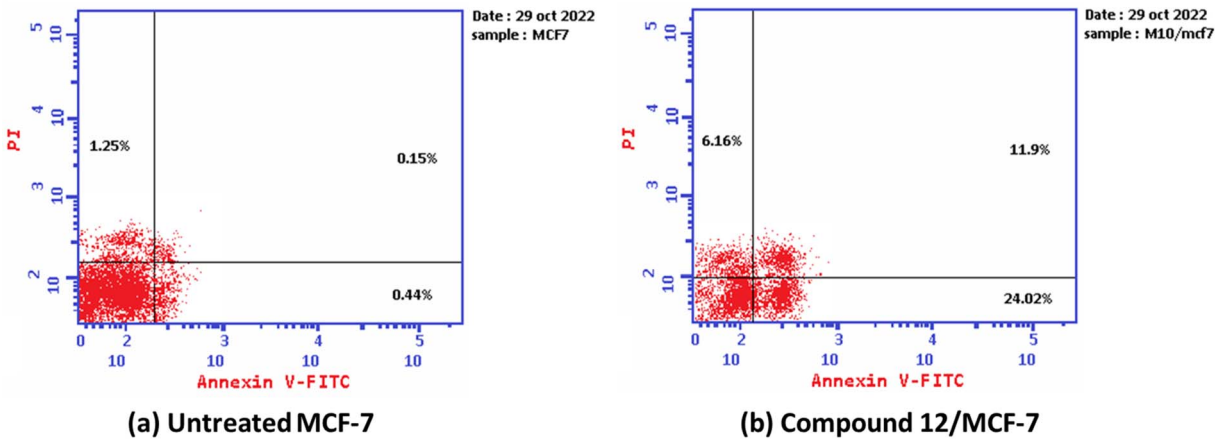

Fig. 3 The graph shows the apoptosis-inducing effects of the most active derivative 12 in MCF-7 when treated at its IC_{50} for 24 h (a) untreated cell; (b) compound 10/MFC-7.

using the RT-PCR technique. Additionally, it is known that Bcl-2 family members, particularly the pro-apoptotic Bax and anti-apoptotic Bcl-2 genes, play a crucial role in controlling apoptosis.[80,81]

As described in Table 3, the 1,3-dithiolo[4,5-*b*]quinoxaline derivative **12** exhibited down-regulation to Bcl-2 protein with 0368 folds compared to untreated MCF-7 cells. At the same time, it revealed activation to pro-apoptotic genes Bax and P53 with 3.97 and 4.97 folds, respectively. Finally, MCF-7 cells' growth rate was significantly reduced by these changes in expression profiles when treated with compound **12**.

*2.2.2.3 Study the activity of compound **12** on receptor tyrosine kinase proteins (EGFR and VEGFR).* To prove the mechanism of the antiproliferative activity, the *in vitro* inhibitory activity against tyrosine kinase proteins: epidermal growth factor EGFR (wide and mutant), and vascular epidermal growth factor receptor VEGFR2 were evaluated for the most active derivative **12** using ELISA analysis. The results of inhibitory activity for the target compound **12** and positive controls against receptor tyrosine kinase proteins expressed by IC_{50} (μM) and the inhibitory percentage at 10 μM are summarized in Table 4. All the results of the target compound **12** against tested proteins displayed values with sub-micromolar (<0.5 μM).

Firstly, 1,3-dithiolo[4,5-*b*]quinoxaline derivative **12** exhibited the highest potential inhibitory activity against $EGFR^{Wt}$ with IC_{50} value 0.19 ± 0.009 μM and inhibitory% = 85.41, compared to doxorubicin (IC_{50} = 0.349 ± 0.016 μM and inhibitory% = 77.59) but still slightly higher than Erlotinib (IC_{50} = 0.037 ± 0.002 μM and inhibitory% = 92.48). Moreover, compound **12** showed a decrease in the suppression effect with an inhibitory percentage value of 87 and the IC_{50} value of 0.121 ± 0.007 μM against mutant $EGFR^{(L858R)}$ related to erlotinib (IC_{50} = 0.026 ± 0.001 μM and inhibitory% = 93). At the same time, compound **12** effectively inhibited VEGFR2 activity with the IC_{50} value of 0.42 ± 0.021 μM and inhibitory% = 78.92, compared with sorafenib (IC_{50} = 0.035 ± 0.002 μM and inhibitory% = 91.68) Fig. 4.

Finally, the sub-micromolar level of inhibition revealed by the assessment results might indicate that the 1,3-dithiolo[4,5-*b*]quinoxaline derivative **12** may benefit EGFR and VEGFR-2

Table 3 *In vitro* gene expression results of the most active derivative **12** against some pro-apoptotic anti-apoptotic proteins using qRT-PCR

	RT-PCR results fold change		
	pro-apoptotic		anti-apoptotic
Tested cpd	Bax	p53	Bcl-2
12/MCF7	3.792	4.976	0.368
Cont.MCF7	1	1	1

Table 4 Level of $EGFR^{Wt}$, $EGFR^{(L858R)}$, and VEGFR2 following the treatment of MCF-7 cells with the IC_{50} dose of the most active derivative **12** and positive controls

	Enzyme inhibitory activity IC_{50}[a] (μM)					
Cpd no	$EGFR^{Wt}$	Inhibitory%[b]	$EGFR^{(L858R)}$	Inhibitory%[b]	VEGFR2	Inhibitory%[b]
12	0.19 ± 0.009	85.41	0.121 ± 0.007	87	0.42 ± 0.021	78.92
Doxorubicin	0.349 ± 0.016	77.59	—	—	—	—
Erlotinib	0.037 ± 0.002	92.48	0.026 ± 0.001	93	—	—
Sorafenib	—	—	—	—	0.035 ± 0.002	91.68

[a] The data is an average of three independent tests. [b] Inhibitory% at 10 μM.

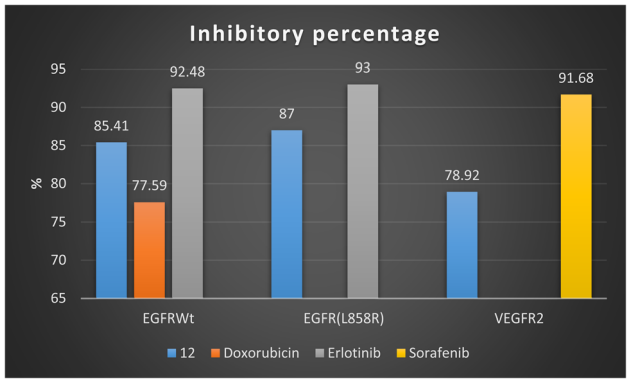

Fig. 4 Inhibitory percentage of 1,3-dithiolo[4,5-*b*]quinoxaline derivative **12** and positive controls (doxorubicin, erlotinib, and sorafenib) against EGFR and VEGFR-2 enzymes.

inhibitory activities with higher inhibitory potency to EGFR-wide and mutant type than VEGFR-2.

2.3. *In silico* ADME and toxicity predictions

2.3.1. Drug likeness and medicinal chemistry prediction. The *in silico* computational evaluation for the most active 1,3-dithiolo[4,5-*b*]quinoxaline derivative **12** and positive controls (doxorubicin, erlotinib, and sorafenib) were evaluated using the SwissADME web tool (**http://swissadme.ch/index.php**, access 15/1/2023) as described previously.[70,82,83] The result of the predicted parameters, including molecular properties, pharmacokinetics, drug-likeness, and medicinal chemistry are presented in Table 5.

The result represented that 1,3-dithiolo[4,5-*b*]quinoxaline derivative **12**, erlotinib, and sorafenib obey both the Lipinski rule of five and Veber rule without any violations, except the doxorubicin that unfollowed the Lipinski rule due to three violations including M. wt over 500 Dalton, hydrogen bond acceptors = 12 (two higher than standard), and hydrogen bond donor = 6 (one more than standard). Additionally, doxorubicin does not follow the Veber rule because the topological polar surface area (TPSA) is higher than 140. Moreover, all the tested compounds exhibited soluble to moderately soluble behaviors with log *S* (ESOL) values ranging from −5.31 to −3.91. Additionally, the most active 1,3-dithiolo[4,5-*b*]quinoxaline derivative **12**, erlotinib, sorafenib demonstrated no pan-assay interference compounds (PAINs) alarms in their structure, while doxorubicin showed only one PAINs alarm due to the quinone ring.

Furthermore, the tested derivative and positive controls revealed acceptable bioavailability scores with values of 0.17 for doxorubicin and 0.55 for the rest of the derivatives. Additionally, compound **12** showed easy synthetic accessibility = 3.75, which is very close to that of erlotinib (3.19) and sorafenib (2.87), as well as less than that of doxorubicin (5.81). Moreover, for pharmacokinetic prediction, all tested derivatives displayed a low gastrointestinal (GI) tract and did not pass the BBB, except erlotinib, which showed high GI and passed the BBB. Also, compound **12** and doxorubicin were revealed to be a substrate for P-gp, which does not cause problems with drug excretion. In

Table 5 Prediction of molecular properties, pharmacokinetics, drug-likeness, and medicinal chemistry of the most active 1,3-dithiolo[4,5-*b*]quinoxaline derivative **12** compared with doxorubicin, erlotinib, and sorafenib

		Most active 1,3-dithiolo[4,5-*b*]quinoxaline derivative **12** and positive controls			
Test items		**12**	Dox.[a]	Erl.[a]	Sor.[a]
SwissADME	**Molecular properties**				
	M log *P*	1.75	−2.10	1.89	2.91
	TPSA (Å^2)	139.21	206.07	74.73	92.35
	M. Wt	433.57	543.52	393.44	464.82
	*n*HBA (NO)	6	12	6	7
	*n*HBD (OHNH)	0	6	1	3
	NRB	2	5	10	9
	Pharmacokinetics				
	GI absorption	Low	Low	High	Low
	BBB permeant	No	No	Yes	No
	P-gp substrate	Yes	Yes	No	No
	Skin permeation (log K_p) cm s^{-1}	−6.69	−8.71	−6.35	−6.25
	Drug likeness and medicinal chemistry				
	log *S* (ESOL)	−4.66	−3.91	−4.11	−5.11
	Solubility	Mod. Soluble	Soluble	Mod. soluble	Mod. soluble
	PAINS	0	1 (quinone)	0	0
	Synthetic accessibility	3.75	5.81	3.19	2.87
	Bioavailability score	0.55	0.17	0.55	0.55
	Lipinski rule (violation)	Yes (0)	No (3)	Yes (0)	Yes (0)
	Veber rule (violation)	Yes (0)	No (1)	Yes (0)	Yes (0)

[a] DOX. = doxorubicin, Erl. = erlotinib, and Sor. = sorafenib.

contrast, erlotinib and sorafenib are not substrates for P-gp. Based on these data, compound **12** appears to be a promising drug candidate for further research and development.

Fig. 5 shows the calculation of the radar charts obtained from the SissADME web tool to predict the accessibility of the tested derivatives to be oral bioavailability. These charts involve six parameters as insaturation (INSATU), polarity (POLAR), insolubility (INSOLU), flexibility (FLEX), lipophilicity (LIPO), and size, and the tested compound is represented by a red line integrated into the pink area. Molecules that fall within the pink region of the radar are considered drug-like. Compound **12** exhibited six of the six rules. At the same time, doxorubicin demonstrated a violation in polarity that related to a number of hydrogen bond donors and acceptors, as well as TPSA > 140, which showed a slight violation to flexibility and that related to the number of rotatable bonds. Moreover, sorafenib demonstrated INSAT violation, which refers to the ratio of hybridized sp^3 atoms to the total number of C atoms.

2.3.2. Toxicological studies. The toxicity prediction for the most active compound and positive control were predicted using two different web tools, such as Protox II (**https://tox-new.charite.de/protox_II/** access 15/1/2023)[84,85] and pkCSM (**https://biosig.lab.uq.edu.au/pkcsm/prediction/** access 15/1/2023) described previously.[86,87] The promising 1,3-dithiolo[4,5-*b*]quinoxaline derivative **12** revealed a median lethal dose (LD_{50} = 420 mg kg^{-1} and belongs to toxicity class IV) higher than doxorubicin (LD_{50} = 205 mg kg^{-1}, class III) and erlotinib (LD_{50} = 125 mg kg^{-1}, class III), while less than sorafenib (LD_{50} = 800 mg kg^{-1}, class IV). The median lethal dose can be described as the amount of substance that gives all at once. Additionally, compound **12** and doxorubicin demonstrated non-toxic to organ toxicity (hepatotoxic) with a probability value of 0.59 and 0.86, respectively. In contrast, erlotinib and sorafenib showed active hepatotoxic activity with probability values of 0.75 and 0.85. Moreover, compound **12** exhibited inactive toxicity endpoint profiles (carcinogenicity, immunotoxicity, mutagenicity, and cytotoxicity) with probability values of 0.67, 0.99, 0.68, and 0.65, respectively.

On the other hand, the positive controls showed activity to immunotoxin, mutagenic, and cytotoxicity, except sorafenib, which displayed inactive to mutagenicity. Additionally, all the tested derivatives were inactive to heat shock factor response element (HSE) with probability values ranging between 0.91 and 0.96 and inactive to mitochondrial membrane potential (MMP) with a probability value ranging between 0.56–0.78, except sorafenib, which displayed activity with a probability of 0.79. In addition, compound **12** and erlotinib depicted inactive tumor suppressor phosphoprotein (p53) with probabilities of 0.88 and 0.89, respectively, and showed activity for doxorubicin and sorafenib (Table 6).

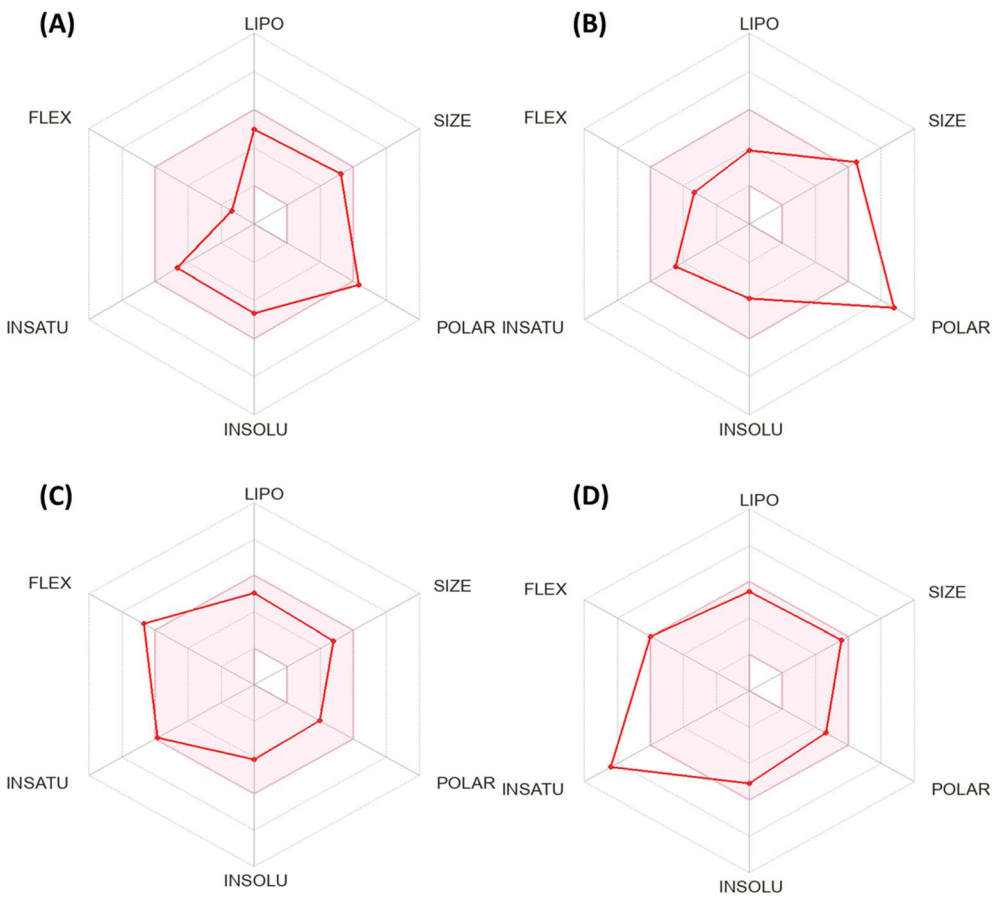

Fig. 5 Bioavailability radar chart generated by Swiss-ADME for (A) the most active compound 12, (B) doxorubicin, (C) erlotinib, and (D) sorafenib.

Table 6 *In silico* toxicity prediction of the most active 1,3-dithiolo[4,5-*b*]quinoxaline derivative **12** compared with doxorubicin, erlotinib, and sorafenib

		Most active 1,3-dithiolo[4,5-*b*]quinoxaline derivative 12 and positive controls			
Oral toxicity prediction		12	Dox.[a]	Erl.[a]	Sor.[a]
Oral toxicity prediction					
ProTox-II prediction	LD_{50} mg kg^{-1}	420	205	125	800
	Toxicity class	IV	III	III	IV
	Hepatotoxicity	Inactive	Inactive	Active	Active
		0.59	0.86	0.78	0.82
	Carcinogenicity	Inactive	Inactive	Inactive	Inactive
		0.67	0.90	0.51	0.50
	Immunotoxicity	Inactive	Active	Active	Active
		0.99	0.99	0.91	0.92
	Mutagenicity	Inactive	Active	Active	Inactive
		0.68	0.98	0.55	0.79
	Cytotoxicity	Inactive	Active	Active	Active
		0.65	0.94	0.75	0.77
	Heat shock factor response element (HSE)	Inactive	Inactive	Inactive	Inactive
		0.91	0.98	0.96	0.96
	Mitochondrial Membrane Potential (MMP)	Inactive	Inactive	Inactive	Active
		0.78	0.56	0.68	0.79
	Phosphoprotein (Tumor suppressor) p53	Inactive	Active	Inactive	Active
		0.88	0.52	0.89	0.57
pkCSM prediction	AMES toxicity	No	Yes	No	No
	Skin sensitisation	No	No	No	No
	hERG I inhibitor	No	No	No	No
	hERG II inhibitor	No	No	Yes	Yes
	Max. tolerated dose (human) (log mg kg^{-1} per day)	−0.042	0.654	0.654	0.677
	Oral rat chronic toxicity (LOAEL) (log mg kg^{-1}_bw per day)	0.973	3.296	1.404	1.054
	Oral rat acute toxicity (LD_{50}) (mol kg^{-1})	3.344	3.978	2.757	2.595

[a] DOX. = doxorubicin, Erl. = erlotinib, and Sor. = sorafenib.

For the pkCSM prediction, all tested derivatives featured non-AMES except doxorubicin, non-skin sensitivity (was not able to elicit an allergic response), and non-inhibitors for hERG I and II (except erlotinib and sorafenib that displayed inhibitor to hERG II). Moreover, the most promising compound **12** expressed the lowest Max. tolerated dose (human) (−0.042 log mg kg^{-1} per day) and oral rat chronic toxicity (LOAEL = 0.973 log mg kg^{-1}_bw per day). Besides, compound **12** showed oral rat acute toxicity (LD_{50} = 3.344 mol kg^{-1}) higher than erlotinib (LD_{50} = 2.757 mol kg^{-1}) and sorafenib (LD_{50} = 2.595 mol kg^{-1}) and lower than doxorubicin (LD_{50} = 3.978 mol kg^{-1}).

Finally, based on the previous toxicity profile, it can be concluded that the most active 1,3-dithiolo[4,5-*b*]quinoxaline derivative **12** exhibited a non-toxic profile on organ toxicity and toxicity endpoints with good LD_{50} value.

2.4. Molecular docking simulations

To determine the suitable anticancer mechanism activity and to explain the experimental result obtained previously, the molecular docking simulation for the most active 1,3-dithiolo [4,5-*b*]quinoxaline derivative **12** was performed inside the active sites of Bcl-2 (PDB: 4AQ3), EGFR (PDB: 1M17), and VEGFR-2 (PDB: 4ASD). All these proteins were downloaded from the protein data bank (https://www.rcsb.org/access 14/1/2023).

2.4.1. Molecular docking study of compound 12 within the Bcl-2 binding pocket. To validate the result of the most active 1,3-dithiolo[4,5-*b*]quinoxaline derivative **12** that displayed downregulation of MCF-7 with 0.368 folds compared with untreated cells. The docking study was performed to identify the binding interactions. Firstly, the human Bcl-2 with sulfonamide inhibitor (PDB: 4AQ3) was downloaded from the protein data bank. Additionally, the validation process was carried out by selecting only one chain and deleting all other chains. Moreover, the redocking process was performed and the co-crystallized ligand (sulfonamide molecule) exhibited binding energy S = −23.39 kcal mol^{-1} with RMSD = 1.49 Å, where the alpha triangle placement and London dG as rescoring functions were selected. The co-crystallized sulfonamide ligand displayed two hydrogen bonds between the Tyr67 with the oxygen of sulfone (SO_2) and NH of sulfonamide with bond lengths of 3.16 Å and 2.18 Å, besides a strength of 11% and 15%, respectively. The docking pose for the most active 1,3-dithiolo[4,5-*b*]quinoxaline derivative **12** exhibited binding energy S = −18.14 kcal mol^{-1} through one hydrogen bond sidechain

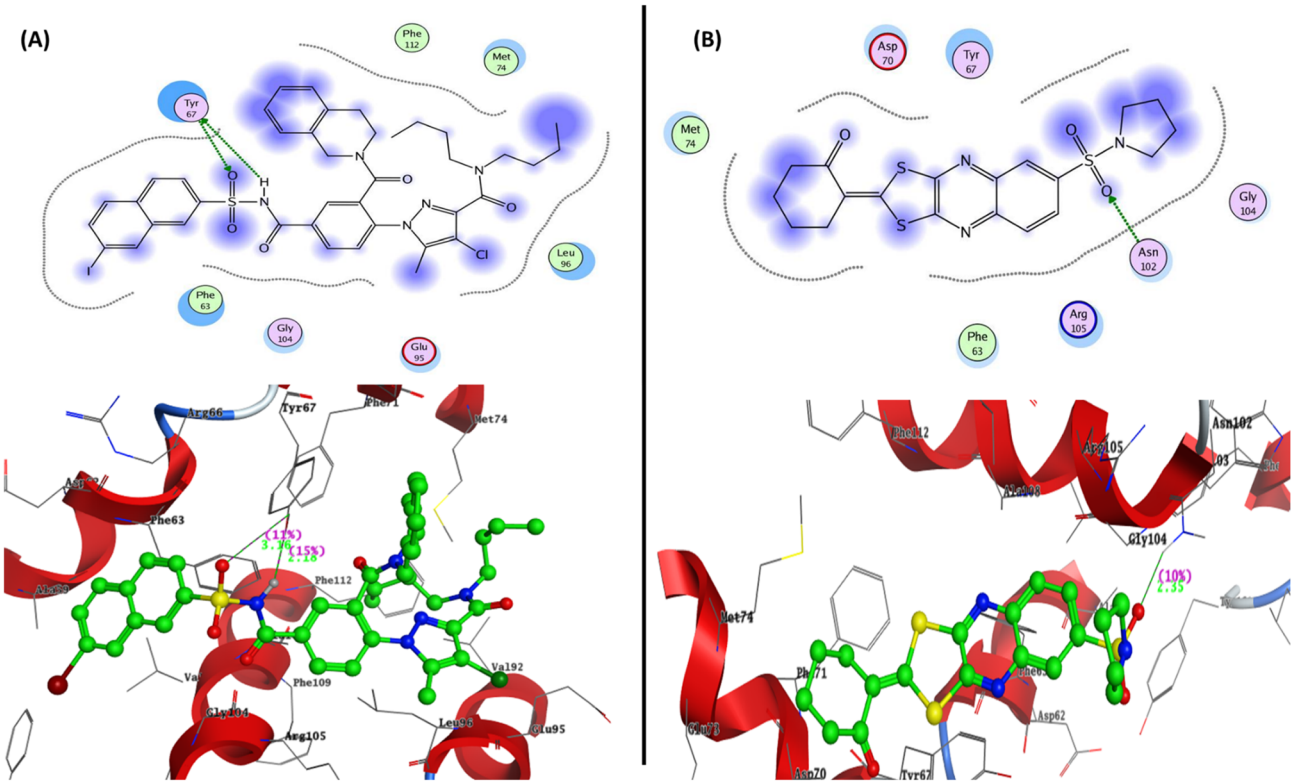

Fig. 6 Represented the 2D and 3D binding modes of (A) co-crystallized ligand and (B) compound **12** inside Bcl-2 binding pocket (PDB: 4AQ3).

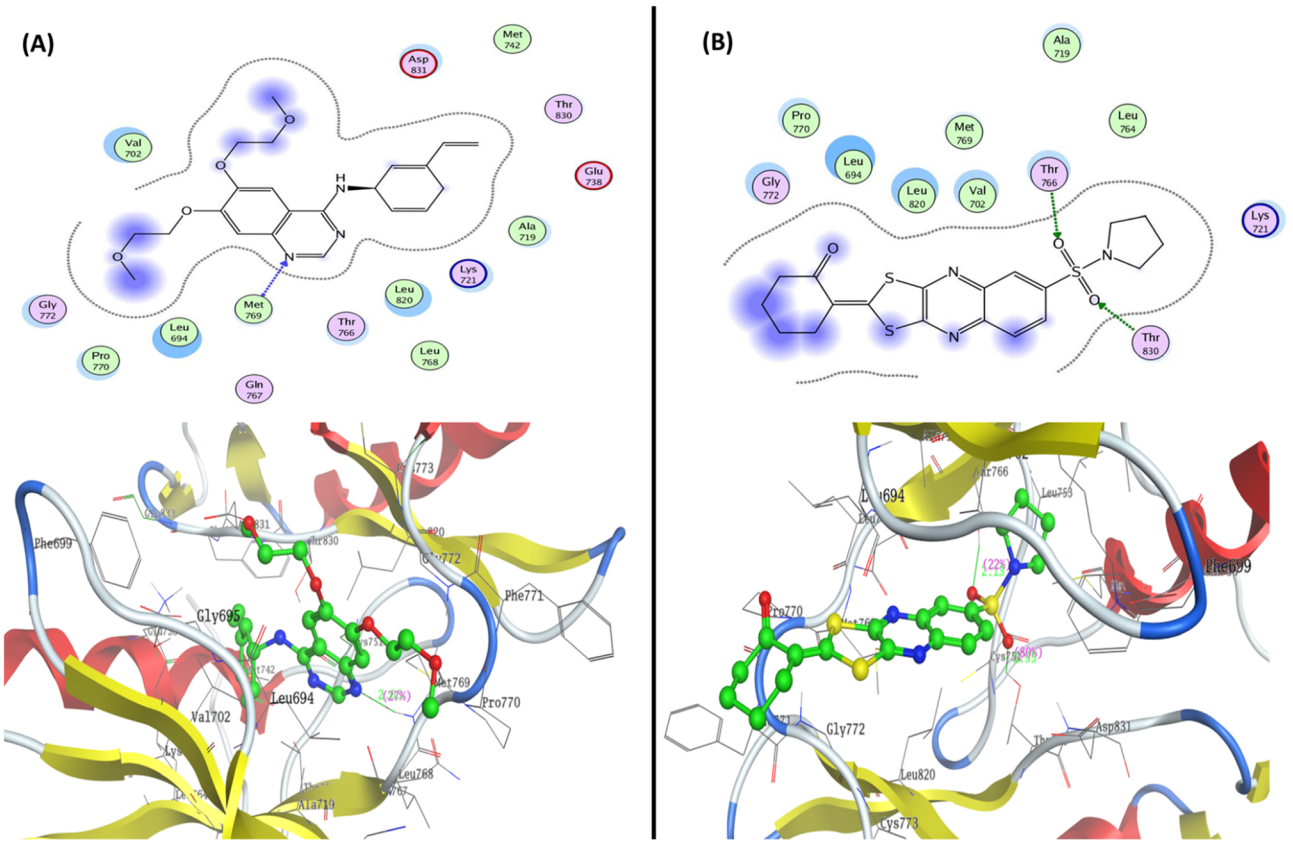

Fig. 7 Represented the 2D and 3D binding modes of (A) co-crystallized ligand and (B) compound **12** inside the EGFR binding pocket (PDB: 1M17).

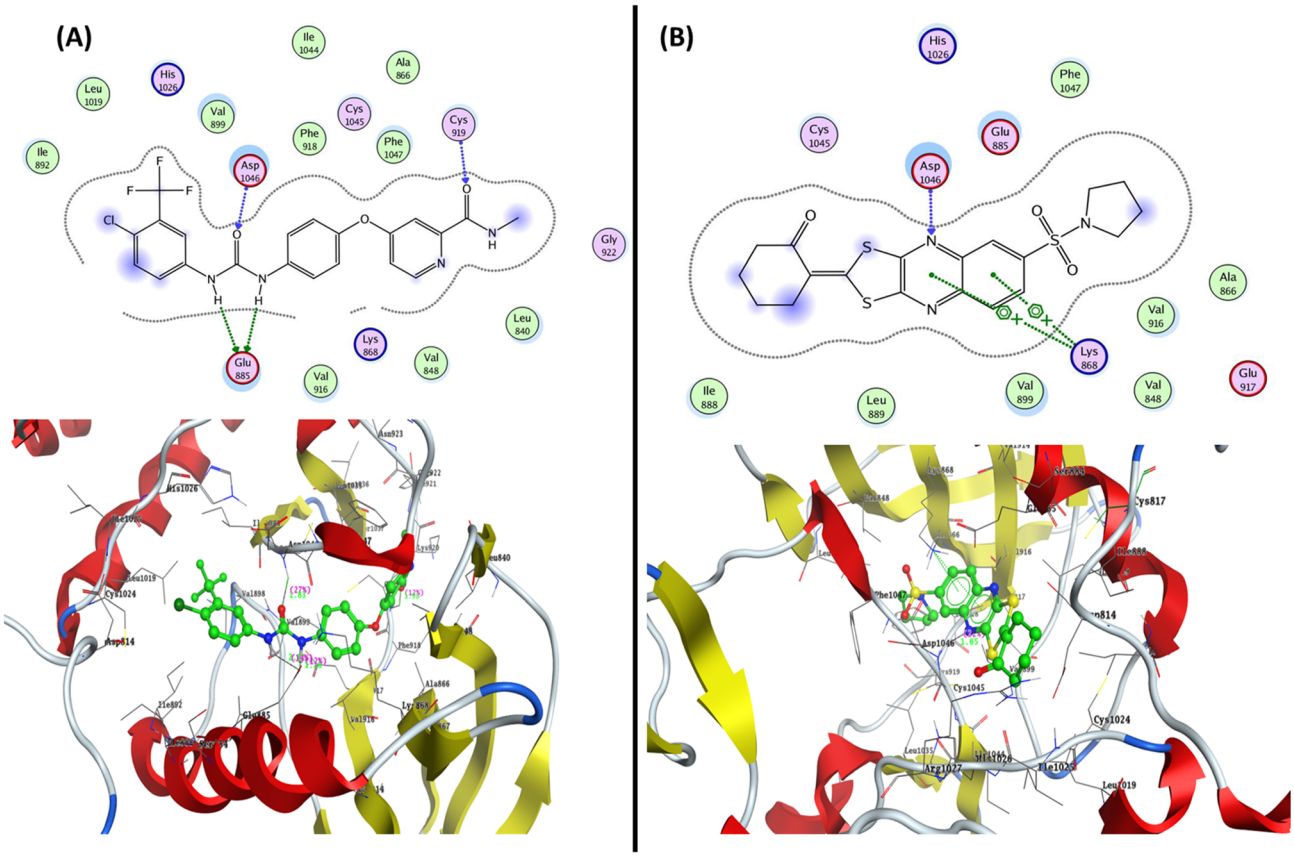

Fig. 8 Represented the 2D and 3D binding modes of (A) co-crystallized ligand and (B) compound **12** inside the VEGFR-2 binding pocket (PDB: 4ASD).

acceptor between Asn102 and oxygen of the sulfone group with bond length 2.35 Å and strength 10% Fig. 6.

2.4.2. Molecular docking study of compound 12 within the EGFR binding pocket. To study the binding pattern for the most active 1,3-dithiolo[4,5-*b*]quinoxaline derivative **12** inside the active site of EGFR (PDB: 1M17), molecular docking simulation was performed in comparison to erlotinib as a positive control (co-crystallized ligand). Compound **12** demonstrated binding energy $S = -16.63$ kcal mol^{-1} through two hydrogen bonds sidechain acceptor between Thr766 and Thr830 with two oxygens of the SO_2 group with bond lengths of 2.13 Å (strength = 22%) and 1.95 Å (strength = 80%), respectively. Moreover, the hydrophobic interaction was observed on the 2-oxo-cyclohexenyl group and over the nitrogen and sulfur of 1,3-dithiolo-quinoxaline derivative. At the same time, erlotinib (co-crystallized ligand) revealed binding energy $S = -17.84$ kcal mol^{-1} with RMSD = 1.73 Å through only one hydrogen bond backbone acceptor between the residue Met769 and nitrogen of quinazoline with a distance of 2.05 Å and strength of 27% Fig. 7.

2.4.3. Molecular docking study of compound 12 within the VEGFR-2 binding pocket. Constructing a molecular docking simulation that can provide the binding mode and correlate experimentally determined IC_{50} values is important. Compound **12** displayed VEGFR inhibitory activity with an IC_{50} value of 0.42 ± 0.021 μM and an inhibitory percentage of 78.92% was docked inside the active site of VEGFR2 (PDB: 4ASD) that contained the sorafenib as co-crystallized ligand. The docking pose displayed one hydrogen bond backbone acceptor between the residue Asp1046 and nitrogen of quinoxaline with a bond length of 1.65 Å and a strength of 22%. Additionally, the phenyl and pyrazine of quinoxaline pharmacophore formed two arene-cation interactions. In contrast, the validation process of sorafenib showed binding energy $S = -16.169$ kcal mol^{-1} with RMSD = 1.484 Å through four hydrogen bonds divided as two hydrogen bond backbone acceptors and two hydrogen bond sidechain donors. The oxygen of the pyridine-2-carboxamide group formed a hydrogen bond backbone acceptor with Cys919 with a bond length of 1.92 Å and strength of 12%, while the oxygen of the carbonyl of urea derivative could form a bond length of 1.83 Å with the strength of 27% with the residue Asp1046. Additionally, the residue Glu885 formed two sidechain hydrogen bond sidechain donors with the two NH groups of the urea derivative with bond lengths of 2.11 and 1.76 Å, as shown in Fig. 8.

3. Conclusion

A series of 1,3-dithiolo[4,5-*b*]quinoxaline derivatives were designed and synthesized based on the hybridization approach between the 2,3-dichloro-6-(pyrrolidin-1-ylsulfonyl)quinoxaline

7 and potassium salt of ethene-1,1-dithiolate derivatives. The designed derivatives contain 1,3-dithiolo[4,5-*b*]quinoxaline derivatives with different fragments and pharmacophores in position two of 2-ylidene-1,3-dithiolanes as the cyclic core and acyclic groups. All the newly designed derivatives were confirmed on the basis of elemental analysis and spectroscopic data. *In vitro* anticancer activity was determined by evaluating the half-maximal inhibitory concentration (IC_{50}) of the synthesized derivative was measured and expressed in μM against HepG-2, HCT-116, and MCF-7 for all the synthesized derivatives. Generally, the tested derivatives exhibited activity in the breast cancer cell line (MCF-7) rather than the colon cell line (HCT-116) and liver cell line (HepG2), with three derivatives exhibiting low micromole against MCF-7 ($IC_{50} \leq 8.78$ μM). Additionally, the most active derivatives **10c**, **10f**, and **12** were tested against other breast cancer cells (MDA-MB-231) and showed significant IC_{50} values ranging from 2.26 ± 0.1 to 10.46 ± 0.8 μM. Moreover, these derivatives showed high cellular cytotoxicity against WI-38 cell lines with IC_{50} values ranging from 46.18 ± 2.4 to 81.64 ± 4.1 μM. Surprisingly, the most active compound **12** exhibited down-regulation to Bcl-2 protein with 0368 folds and caused an activation to pro-apoptotic genes Bax and P53 with 3.97 and 4.97 folds, respectively, compared to untreated MCF-7 cells. Additionally, compound **12** revealed $EGFR^{Wt}$ and $EGFR^{(L858R)}$ with inhibition percentages of 85.41% and 87% at 10 μM, as well as inhibited VEGFR-2 activity with the IC_{50} value of 0.42 ± 0.021 μM and inhibitory% = 78.92, compared with sorafenib (IC_{50} = 0.035 ± 0.002 μM and inhibitory% = 91.68). Further, compound 12 inhibited the growth of MCF-7 cells at its IC_{50} value in the S phase with values of 48.16% compared with the untreated control at 29.79%. Finally, some *in silico* ADMET prediction was performed for the most active compound **12**, and the results exhibited a safety profile with drug-likeness properties. Additionally, the docking simulation inside the active site of Bcl-2, EGFR, and VEGFR-2 was performed and discussed.

4. Experimental

4.1. Chemistry

4.1.1. Materials and instrumentation. All reagents and chemicals were ordered from Aldrich Chemicals and used without further purifications and solvents were obtained from Fisher. Melting points (MPs) of all the newly designed compounds were recorded on a digital Gallen Kamp MFB-595 instrument using open capillaries. IR spectra were collected in the range of 400–4000 cm^{-1} with the KBr disc methodology on a Shimadzu 440 spectrophotometer. For NMR spectra ($^1H/^{13}C$), chemical shifts were calculated in δ ppm relative to TMS as an internal standard (= 0 ppm) from the spectra obtained on a JOEL spectrometer 500/125 MHz using $CDCl_3$ and DMSO-d_6 as solvents. The data are provided in the following format: chemical shift, multiplicity (br. = broad, m = multiplet, qu = quintet, q = quartet, t = triplet, d = doublet, and s = singlet), coupling constant (J) in Hertz (Hz), and integration. Elemental studies were carried out at Cairo University's Micro Analytical Unit in Cairo. At Al-Azhar University's Regional Center for Biotechnology, mass spectra were collected at 70 eV using the DI-50 unit of a Shimadzu GC/MSQP5050A spectrometer. The anticancer activity, including the cell lines (HepG2, HCT-116, MCF-7, MDA-MB-231, and WI-38) and enzymes assays were performed at VACSERA Tissue Culture Unit, Cairo, Egypt. 1,4-dihydroquinoxaline-2,3-dione **2** and 2,3-dioxo-1,2,3,4-tetrahydroquinoxaline-6-sulfonyl chloride (**3**) were prepared according to the literature methods.[74–76]

4.1.2. Synthesis of organic materials

4.1.2.1 Synthesis of 6-(pyrrolidin-1-ylsulfonyl)-1,4-dihydroquinoxaline-2,3-dione (5). A solution of sulfonyl chloride derivative, **3** (1 mmol) in 1,4-dioxane (25 mL), and pyrrolidine **4** (1.5 mmol) as a secondary amine was added dropwise for 15 min at room temperature. The solution mixture was stirred 15 min at room temperature for a further 5 h (monitored by TLC). After the new product was precipitated, the precipitate was collected by filtration and crystallized from EtOH to obtain the required product.

Pale-white powder (EtOH); 88% Yield; M.p. = 275–277 °C; IR (KBr): ν_{max} = 3502, 3366 (2NH), 3046 (CH_{ar}), 2959, 2922 (CH_{alip}), 1692 (br. 2C=O), 1613 (C=N), 1330, 1148 (SO_2) cm^{-1}; ^1H NMR (δ, ppm) = 1.67 (4H, qu, $2CH_2$·pyrolidine), 3.25 (4H, t, 2N–CH_2·pyrolidine), 8.24 (d, 1H, J = 8.0 Hz, H_7·quinox), 8.28 (d, 1H, J = 8.0 Hz, H_8·quinox), 8.41 (s, 1H, H_5·quinox), 11.97 (2H, s, 2NH: D_2O exchangeable); ^{13}C NMR (δ, ppm) = 25.10 ($2CH_2$·pyrolidine), 48.31 (2N–CH_2·pyrolidine), 124.94, 126.16, 127.68, 130.03, 138.99, 139.53 (Ar.Cs), 167.44 (2CO); Anal. Calcd for $C_{12}H_{13}N_3O_4S$ (295.31): C, 48.81; H, 4.44; N, 14.23; Found: C, 48.65; H, 4.12; N, 14.54.

4.1.2.2 Synthesis of 2,3-disubstituted-6-(pyrrolidin-1-ylsulfonyl)quinoxaline (6 and 7). DMF (2 mL) was added drop by drop to a solution of 6-(pyrrolidin-1-ylsulfonyl)-1,4-dihydroquinoxaline-2,3-dione **2** (4 mmol) and trichlorophosphate (10 mmol), the solution was stirred at 80 °C for 2 h to precipitate the monochloro derivatives **6**. After adding excess trichloro-phosphate (10 mmol) and stirring at 80 °C for 4 h, the previously formed precipitate disappeared and the solution becomes viscous (monitored by TLC). After the reaction was completed, the solution was added portion-wise to ice water and neutralized with an ammonia solution, 30%. The formed precipitate was collected by filtration and crystallized from CH_3CN to obtain the dichloro derivatives **7**.

4.1.2.3 3-Chloro-6-(pyrrolidin-1-ylsulfonyl)quinoxalin-2(1H)-one (6). Pale-brown powder (CH_3CN); 81% Yield; M.p. = 240–242 °C; IR (KBr): ν_{max} = 3401 (NH), 3063 (CH_{ar}), 2956, 2897 (CH_{alip}), 1694 (CO), 1555(C=N), 1344, 1150 (SO_2) cm^{-1}; ^1H NMR (δ, ppm) = 1.91 (4H, qu, $2CH_2$·pyrolidine), 3.75 (4H, t, 2N–CH_2·pyrolidine), 7.94 (d, 1H, J = 9.7 Hz, H_7·quinox), 8.08 (d, 1H, J = 9.2 Hz, H_8·quinox), 8.11 (s, 1H, H_5·quinox); ^{13}C NMR (δ, ppm) = 25.29 ($2CH_2$·pyrolidine), 50.19 (2N–CH_2·pyrolidine), 125.00, 127.93, 130.33, 131.79, 135.98, 140.06 (Ar.Cs), 144.65 (N=C–Cl), 164.59 (C=O); Anal. Calcd. for $C_{12}H_{12}ClN_3O_3S$ (313.76): C, 45.94; H, 3.86; N, 13.39; Found: C, 45.78; H, 3.92; N, 13.42.

4.1.2.4 2,3-Dichloro-6-(pyrrolidin-1-ylsulfonyl)quinoxaline (7). Grey powder (CH_3CN); 85% Yield; M.p. = 190–192 °C; IR (KBr): ν_{max} = 3051(CH_{ar}), 2970, 2875 (CH_{alip}), 1615 (C=N), 1336, 1151

(SO_2) cm^{-1}; ^1H NMR (δ,ppm) = 1.63 (4H, qu, $2CH_2$·pyrrolidine), 3.26 (4H, t, 2N–CH_2·pyrolidine), 8.22 (d, 1H, J = 8.0 Hz, H_7-·quinox), 8.28 (d, 1H, J = 8.0 Hz, H_8·quinox), 8.42 (s, 1H, H_5-·quinox); ^{13}C NMR (δ, ppm) = 25.10 ($2CH_2$·pyrrolidine), 48.31 (2N–CH_2·pyrolidine), 125.99, 127.68, 130.03, 138.99, 139.53 (Ar.Cs), 141.78 (C–SO_2), 147.09 (N=C–Cl), 147.77 (N=C–Cl); Anal. Calcd for $C_{12}H_{11}ClN_3O_2S$ (332.20): C, 43.39; H, 3.34; N, 12.65; Found: C, 43.46; H, 3.78; N, 12.21.

*4.1.2.5 A general method for the preparation of potassium ethene-1,1-dithiolates anion (**9**).* A mixture of active methylene compound **8** (0.01 mmol), carbon disulfide (0.01 mmol), and potassium hydroxide (0.02 mmol) in absolute ethanol (15 mL) was stirred at room temperature for 30 min. The resulting solid product was collected by filtration, and washed with ether to obtain the desired disulphide anion (**9**).

*4.1.2.6 Synthesis of substituted 2-ylidene-6-(pyrrolidin-1-ylsulfonyl)-[1,3]dithiolo[4,5-b]quinoxalines (**10a–f**).* **General method**: In a 100 mL bottom conical flask, a solution of 2,3-dichloro-6-(pyrrolidin-1-ylsulfonyl)quinoxaline (2 mmol) (**7**) in a little amount of dimethylformamide as a solvent, and substituted potassium ethene-1,1-bis(thiolates) **9** (2 mmol) were added. The reaction mixture was stirred at room temperature for 2–6 h (monitored by TLC). After the reaction was completed, the precipitate was filtered off and recrystallized from the proper solvent to produce the desired pure solid **10a–i**. The spectroscopic data of all prepared compounds are listed below.

*4.1.2.7 2-(6-(Pyrrolidin-1-ylsulfonyl)-[1,3]dithiolo[4,5-b] quinoxalin-2-ylidene)malononitrile (**10a**).* Yellow powder (CH_3CN); 86% Yield; M.p. = 230–232 °C; IR (KBr): ν_{max} = 3072 (CH_{ar}), 2971, 2878 (CH_{alip}), 2219, 2193 (2CN), 1621 (C=N), 1550 (C=C), 1334, 1150 (SO_2) cm^{-1}; ^1H NMR (δ, ppm) 1.65 (4H, qu, $2CH_2$·pyrolidine), 3.25 (4H, t, 2N–CH_2·pyrrolidine), 8.24 (1H, dd, J = 6.4, 2.0 Hz, H_7·quinox), 8.31 (1H, d, J = 8.8 Hz, H_8-·quinox), 8.43 (1H, s, H_5·quinox); ^{13}C NMR (δ, ppm) = 25.53 ($2CH_2$·pyrolidine), 48.44 (2N–CH_2·pyrolidine), 88.87 (C–CN), 111.92 (2CN), 128.14, 128.90, 130.45, 138.80, 139.19, 141.27, 149.74, 150.42 (C_{arom}), 173.46 (S–C=C); MS: (M_{wt}: 401): m/z, 401 [M^+, (16.41%)], 317.44 (100%); Anal. Calcd for $C_{16}H_{11}N_5O_2S_3$ (401.48): C, 47.87; H, 2.76; N, 17.44; Found: C, 47.61; H, 2.55; N, 17.33.

*4.1.2.8 Ethyl 2-cyano-2-(6-(pyrrolidin-1-ylsulfonyl)-[1,3] dithiolo[4,5-b]quinoxalin-2-ylidene)acetate (**10b**).* Light-yellow powder (CH_3CN); 67% Yield; M.p. = 233–235 °C; IR (KBr): ν_{max} = 3075 (CH_{ar}), 2977, 2875 (CH_{alip}), 2211 (CN), 1691 (CO), 1605 (C=N), 1553 (C=C), 1345, 1152 (SO_2) cm^{-1}; ^1H NMR (δ, ppm) = 1.33 (3H, t, CH_3·ester), 1.67 (4H, qu, $2CH_2$·pyrrolidine), 3.27 (4H, t, 2N–CH_2·pyrolidine), 4.37 (2H, q, CH_2·ester), 8.15 (1H, dd, J = 8.8, 2.4 Hz, H_7·quinox), 8.29 (1H, d, J = 8.8 Hz, H_8·quinox), 8.29 (1H, s, H_5·quinox); ^{13}C NMR (δ, ppm) = 14.02 (CH_3·ester), 24.94 ($2CH_2$·pyrolidine), 48.17 (2N–CH_2-·pyrolidine), 62.72 (CH_2·ester), 92.39 (C–CN), 114.45 (CN), 122.33, 125.06, 126.40, 136.68, 137.17, 138.16, 149.95, 151.26 (C_{arom}), 165.86 (CO. ester), 167.57 (S–C=C); Anal. Calcd for $C_{18}H_{16}N_4O_4S_3$ (448.53): C, 48.20; H, 3.60; N, 12.49; Found: C, 48.10; H, 3.55; N, 12.30.

*4.1.2.9 2-Cyano-2-(6-(pyrrolidin-1-ylsulfonyl)-[1,3]dithiolo [4,5-b]quinoxalin-2-ylidene)-N-(3-(trifluoromethyl)phenyl) acetamide (**10c**).* Deep-yellow powder (CH_3CN); 67% Yield; M.p. = 161–163 °C; IR (KBr): ν_{max} = 3342 (br. OH), 3046 (CH_{ar}), 2950, 2922 (CH_{alip}), 2224 (CN), 1592 (C=O), 1511 (C=C), 1329, 1150 (SO_2) cm^{-1}; ^1H NMR (δ, ppm) = 1.67 (4H, qu, $2CH_2$·pyrolidine), 3.18 (4H, t, 2N–CH_2·pyrrolidine), 7.17 (1H, d, J = 8.0, H_{arom}), 7.69–7.71 (1H, m, H_{arom}), 7.81 (1H, d, J = 9.6 Hz, H_{arom}), 7.88 (dd, 1H, J = 8.7, 2.1 Hz, H_7·quinox), 7.92 (1H, s, H_{arom}), 8.07 (1H, d, J = 6.8 Hz, H_8·quinox), 8.10 (1H, s, H_5·quinox), 9.87 (1H, s, NH: exchangeable by D_2O); ^{13}C NMR (δ, ppm) = 24.80 ($2CH_2$·pyrolidine), 48.33 (2N–CH_2·pyrolidine), 88.27 (C–CN), 115.01 (CN), 123.37, 123.50, 124.65 (C–F_3), 125.57, 127.37, 129.66, 132.89, 133.40, 134.04, 136.58, 137.92, 139.30, 151.23, 151.42 (C_{arom}), 163.44 (C–NH), 170.67 (S–C=C); MS: m/z, 563 [M+, (23.45%)], 198.35 (100%); Anal. Calcd for $C_{23}H_{16}F_3N_5O_3S_3$ (563.59): C, 49.02; H, 2.86; N, 12.43; Found: C, 49.01; H, 2.76; N, 12.35.

*4.1.2.10 2-Cyano-N′-(4-methoxybenzylidene)-2-(6-(pyrrolidin-1-ylsulfonyl)-[1,3]dithiolo[4,5-b]quinoxalin-2-ylidene) acetohydrazide (**10d**).* Yellow powder (CH_3CN); 73% Yield; M.p. = 145–147 °C; IR (KBr): ν_{max} = 3442, 3333 (br. OH), 3046 (CH_{ar}), 2950, 2881 (CH_{alip}), 2198 (CN), 1603 (C=O), 1552 (C=C), 1332, 1148 (SO_2) cm^{-1}; ^1H NMR (δ, ppm) 1.66 (4H, qu, $2CH_2$-·pyrolidine), 3.18 (4H, t, 2N–CH_2·pyrrolidine), 3.69 (3H, s, CH_3·methoxy), 7.60 (2H, d, J = 9.2H, H_{arom}), 7.69–7.73 (2H, m, H_{arom}), 7.90–7.93 (1H, m, H_7·quinox), 8.07 (1H, d, J = 7.2 Hz, H_8·quinox), 8.16 (1H, s, H_5·quinox), 11.38 (1H, s, NH: exchangeable); ^{13}C NMR (δ, ppm) = 24.60 ($2CH_2$·pyrolidine), 47.84 (2N–CH_2·pyrolidine), 54.63 (OCH_3) 86.10 (C–CN), 115.56 (CN), 122.90, 123.59, 124.51, 125.56, 127.14, 129.84, 130.25, 130.63, 134.21, 136.04, 139.24, 144.07, 151.24, 151.72 (C_{arom}), 161.31 (C–NH), 165.53 (C–OMe), 170.90 (S–C=C); Anal. Calcd for $C_{25}H_{20}N_5O_4S_3$ (550.65): C, 54.53; H, 3.66; N, 12.72; Found: C, 54.43; H, 3.54; N, 12.47.

*4.1.2.11 2-Cyano-N′-(2-oxoindolin-3-ylidene)-2-(6-(pyrrolidin-1-ylsulfonyl)-[1,3]dithiolo[4,5-b]quinoxalin-2-ylidene) acetohydrazide (**10e**).* Brown powder (CH_3CN); 91% Yield; M.p. = 310–312 °C; IR (KBr): ν_{max} = 3418 (2NH), 3046 (CH_{ar}), 2955 (CH_{alip}), 2202 (CN), 1718 (CO), 1675 (CO), 1618 (C=N), 1545 (C=C), 1331, 1149 (SO_2) cm^{-1}; ^1H NMR (δ, ppm) 1.66 (4H, qu, $2CH_2$·pyrolidine), 3.16 (4H, t, 2N–CH_2·pyrrolidine), 7.35 (1H, t, J = 8.4 Hz, H_{arom}), 7.47 (1H, t, J = 6.8 Hz, H_{arom}), 7.55–7.70 (2H, m, H_{arom}), 7.72 (1H, d, J = 8.8 Hz, H_7·quinox), 7.95 (1H, d, J = 10.8 Hz, H_8·quinox), 8.50 (1H, s, H_5·quinox), 11.24 (1H, s, NH: exchangeable with D_2O), 12.42 (1H, s, NH: exchangeable with D_2O); ^{13}C NMR (δ, ppm) = 25.27 ($2CH_2$·pyrolidine), 50.21 (2N–CH_2·pyrolidine), 95.17 (C–CN), 114.24 (CN), 120.04, 121.24, 124.96, 125.40, 127.15, 130.30, 131.77, 133.73, 135.89, 137.06, 141.58, 142.62, 144.58, 148.48, 148.79 (C_{arom}), 160.61 (CO), 164.04 (CO), 168.66 (S–C=C); Anal. Calcd for $C_{24}H_{17}N_7O_4S_3$ (563.63): C, 51.14; H, 3.04; N, 17.40; Found: C, 51.01; H, 3.00; N, 17.12.

*4.1.2.12 Ethyl 3-oxo-2-(6-(pyrrolidin-1-ylsulfonyl)-[1,3]dithiolo [4,5-b]quinoxalin-2-ylidene)butanoate (**10f**).* Brown powder (CH_3CN); 77% Yield; M.p. = 217–219 °C; IR (KBr): ν_{max} = 3046 (CH_{ar}), 2984, 2957 (CH_{alip}), 1714 (br.CO), 1626 (C=N), 1576 (C=C), 1328, 1149 (SO_2) cm^{-1}; ^1H NMR (δ, ppm) = 1.43 (3H, t,

CH_3·ester), 1.65 (4H, qu, $2CH_2$·pyrolidine), 2.49 (3H, s, CH_3-·acetyl), 3.20 (4H, t, 2N–CH_2·pyrolidine), 4.51 (2H, q, CH_2-·ester), 7.85 (1H, dd, $J = 4.7$, 1.6 Hz, H_7·quinox), 7.87 (1H, d, $J =$ 8.4 Hz, H_8·quinox), 8.02 (1H, s, H_5·quinox); ^{13}C NMR (δ, ppm) = 14.07 (CH_3·ester), 24.28 ($2CH_2$·pyrolidine), 28.77 (CH_3·acetyl), 48.11 (2N–CH_2·pyrolidine), 63.15 (CH_2·ester), 109.60, 124.52, 125.61, 127.35, 132.89, 136.11, 139.37, 150.64, 150.98 (C_{arom}), 165.18 (CO.ester), 170.00 (S–C=C), 187.32 (CO.acetyl); MS: *m*/*z*, 465 [M^+, (16.99%)], 246.20 (100%); Anal. Calcd for $C_{19}H_{19}N_3O_5S_3$ (465.56): C, 49.02; H, 4.11; N, 9.03; Found: C, 49.01; H, 4.10; N, 9.01.

*4.1.2.13 Synthesis of novel [1,3]dithiolo[4,5-b]quinoxaline linked to cyclohexyl, pyrazolyl, and pyrimidinyl moieties (**12**, **14**, **16**, and **18**).* In a 100 mL bottom conical flask, a solution of the starting material 2,3-dichloro-6-(pyrrolidin-1-ylsulfonyl) quinoxaline (**7**) (2 mmol) in a little amount of DMF as a solvent, and substituted potassium ethene-1,1-bis(thiolates) (2 mmol) specific namely, potassium (2-oxocyclohexylidene) methanebis(thiolate) (**11**), potassium (3-methyl-5-oxo-1,5-dihydro-4*H*-pyrazol-4-ylidene)methanebis(thiolate) (**13**), potassium (3-methyl-5-oxo-1-phenyl-1,5-dihydro-4*H*-pyrazol-4-ylidene) methanebis(thiolate) (**15**), and potassium (2,4,6-trioxotetrahydropyrimidin-5(2*H*)-ylidene)methanebis(thiolate) (**17**) were added. The reaction mixture was stirred at room temperature for 3–7 h (monitored by TLC). After the reaction was completed, the precipitate was filtered off and recrystallized from the proper solvent to produce the desired pure solid. The spectroscopic data of all prepared compounds are listed below.

*4.1.2.14 2-(6-(Pyrrolidin-1-ylsulfonyl)-[1,3]dithiolo[4,5-b] quinoxalin-2-ylidene)cyclohexan-1-one (**12**).* Deep-yellow (CH_3CN); 80% yield; M.p. 176–178 °C; IR (KBr): ν_{max} = 3073 (CH_{ar}), 2972, 2923, 2880 (CH_{alip}), 1654 (CO), 1602 (C=N), 1545 (C=C), 1330, 1151 (SO_2) cm^{-1}; ^{1}H NMR (δ, ppm) = 1.43 (2H, t, CH_2·hex), 1.62–1.65 (6H, m, $2CH_2$·pyrrolidine + CH_2·hex), 2.61 (2H, s, CH_2·hex), 3.16–3.20 (6H, m, 2N–CH_2·pyrrolidine + CH_2·hex), 7.87 (1H, d, $J = 8.0$ Hz, H_7·quinox), 7.92 (1H, d, $J =$ 10.4, H_8·quinox), 8.02 (1H, s, H_5·quinox); ^{13}C NMR (δ, ppm) = 18.63 (CH_2·hex), 22.85 (CH_2·hex), 24.92 ($2CH_2$·pyrolidine), 27.83 (CH_2·hex), 37.66 (CH_2·hex), 47.93 (2N–CH_2·pyrolidine), 117.40 (C–CO), 123.78, 124.44, 125.57, 127.32, 130.12, 134.18, 136.09, 139.24, 151.20, 151.53 (C_{arom}), 163.37 (S–C=C), 178.00 (CO); MS: *m*/*z*, 433 [M^+, (30.54%)], 73.30 (100%); Anal. Calcd for $C_{19}H_{19}N_3O_3S_3$ (433.56): C, 52.64; H, 4.42; N, 9.69; Found: C, 52.44; H, 4.27; N, 9.23.

*4.1.2.15 5-Methyl-4-(6-(pyrrolidin-1-ylsulfonyl)-[1,3]dithiolo [4,5-b]quinoxalin-2-ylidene)-2,4-dihydro-3H-pyrazol-3-one (**14**).* Light-yellow (CH_3CN); 68% Yield; M.p. = 225–227 °C; IR (KBr): ν_{max} = 3117 (NH), 3064 (CH_{ar}), 2956, 2925 (CH_{alip}), 1670 (CO), 1525 (C=C), 1340, 1150 (SO_2) cm^{-1}. ^{1}H NMR (δ, ppm) = 1.69 (4H, qu, $2CH_2$·pyrolidine), 2.39 (3H, s, CH_3·pyrazole), 3.27 (4H, t, 2N–CH_2·pyrrolidine), 8.19 (1H, dd, $J = 11.6$, 3.6, H_7·quinox), 8.27 (1H, d, $J = 8.8$ Hz, H_8·quinox), 8.30 (1H, s, H_5·quinox), 11.58 (1H, s, NH: exchangeable with D_2O); ^{13}C NMR (δ, ppm) = 14.54 (CH_3·pyrazole), 25.74 ($2CH_2$·pyrolidine), 50.61 (2N–CH_2-·pyrolidine), 103.72 (C–CO), 128.34, 130.73, 132.22, 136.37, 137.46, 140.62, 145.02, 149.27, 152.61 (C_{arom}), 169.17 (S–C=C), 177.76 (CO.pyrazole); Anal. Calcd for $C_{17}H_{15}N_5O_3S_3$ (433.52): C, 47.10; H, 3.49; N, 16.16; Found: C, 47.01; H, 3.38; N, 16.05.

*4.1.2.16 5-Methyl-2-phenyl-4-(6-(pyrrolidin-1-ylsulfonyl)-[1,3] dithiolo[4,5-b]quinoxalin-2-ylidene)-2,4-dihydro-3H-pyrazol-3-one (**16**).* Orange powder (CH_3CN); 73% Yield; M.p. = 240–242 °C; IR (KBr): ν_{max} = 3062, 3045 (CH_{ar}), 2980, 2948 (CH_{alip}), 1705 (CO), 1641 (C=N), 1593 (C=C), 1320, 1150 (SO_2) cm^{-1}; ^{1}H NMR (δ, ppm) 1.68 (4H, qu, $2CH_2$·pyrolidine), 2.44 (3H, s, CH_3, pyrazole), 3.25 (4H, t, 2N–CH_2·pyrrolidine), 7.20–7.27 (1H, m, H_{arom}), 7.47 (2H, t, $J = 7.2$ Hz, H_{arom}), 7.92 (1H, d, $J = 8.0$, H_7-·quinox), 8.12 (2H, d, $J = 6.8$, H_{arom}), 8.18 (1H, d, $J = 8.4$, H_8-·quinox), 8.30 (1H, s, H_5·quinox); ^{13}C NMR (δ, ppm) = 15.19 (CH_3·pyrazole), 26.48 ($2CH_2$·pyrolidine), 50.63 (2N–CH_2-·pyrrolidine), 103.05 (C–CO), 124.24, 124.44, 125.65, 126.60, 126.82, 128.05, 128.76, 131.10, 132.30, 136.58, 139.88, 140.57, 147.58, 149.36, 149.81 (C_{arom}), 166.17 (S–C=C), 175.51 (CO.pyrazole); MS: *m*/*z*, 509 [M^+, (22.35%)], 229.15 (100%); Anal. Calcd for $C_{23}H_{19}N_5O_3S_3$ (509.62): C, 54.21; H, 3.76; N, 13.74; Found: C, 54.08; H, 3.55; N, 13.69.

*4.1.2.17 5-(6-(Pyrrolidin-1-ylsulfonyl)-[1,3]dithiolo[4,5-b]quinoxalin-2-ylidene)pyrimidine-2,4,6(1H,3H,5H)-trione (**18**).* Pale-green powder (CH_3CN); 80% Yield; M.p. = 238–240 °C; IR (KBr): ν_{max} = 3502, 3115 (2NH), 3046 (CH_{ar}), 2985, 2917 (CH_{alip}), 1640 (br. 3CO), 1615 (C=N), 1488 (C=C), 1370, 1150 (SO_2) cm^{-1}; ^{1}H NMR (δ, ppm) = 1.65 (4H, s, $2CH_2$·pyrolidine), 3.25 (4H, s, 2N–CH_2·pyrrolidine), 8.25 (1H, d, $J = 9.6$, H_7-·quinox), 8.30 (1H, d, $J = 8.8$, H_8·quinox), 8.42 (1H, s, H_5-·quinox), 11.12 (1H, s, 2NH: exchangeable with D_2O); ^{13}C NMR (δ, ppm) = 25.37 ($2CH_2$·pyrolidine), 48.30 (2N–CH_2·pyrolidine), 105.37 (C–CO), 127.79, 128.91, 130.30, 136.03, 139.44, 140.00, 142.15, 147.37, 147.81, 152.13 (C_{arom}), 157.97 (CO-pyrimidine), 160.41 (2CO-pyrimidine), 168.13 (S–C=C); Anal. Calcd for $C_{17}H_{13}N_5O_5S_3$ (463.50): C, 44.05; H, 2.83; N, 15.11; Found: C, 44.01; H, 2.66; N, 15.04.

4.2. Biological activities

The *in vitro* cytotoxicity screening of the newly designed 6-(pyrrolidin-1-ylsulfonyl)quinoxaline derivatives **7**, **10**, **12**, **14**, **16**, and **18** was performed against three human cancer cell lines (Hep G2, HCT-116, and MCF-7) using MTT assay through incubation period 24 h, as described previously.[37,78] Moreover, the most active derivatives **10c**, **10f**, and **12** were further evaluated against MDA-MB-231 and non-tumorigenic normal cell line (WI-38) using MTT assay. The cell lines were obtained from ATCC *via* the Holding company for biological products and vaccines (VACSERA), Cairo, Egypt (the principle of MTT assay and standard protocol are shown in the ESI,† including all steps). Moreover, the *in vitro* flow cytometry cell cycle analysis, and apoptosis annexin V-FITC Apoptosis Detection BioVision Kit were performed at the VACSERA Tissue Culture Unit, Cairo, Egypt, as described previously.[33] The effect of most active derivative **12** on the gene expression of Bcl-2, Bax, and P53 was determined using qRT-PCR using the Bio-Rad Laboratories iScript TM One-Step RT-PCR Kit with SYBR® Green according to manufacturer's instructions and as described previously.[88] Additionally, the *in vitro* EGFR ^{wt}, EGFR ^{L858R}, and VEGFR for

the most active derivative **12** were performed using the BPS-Bioscience EGFR Kinase Assay Kit Catalog #40321, EGFR(L858R) Kinase Assay Kit Catalog #40324, and VEGFR-2(KDR) Kinase Assay Kit Catalog #40325, respectively, according to the manufacturer's instructions.

4.3. Molecular docking simulations

The molecular docking studies for the most active 1,3-dithiolo [4,5-*b*]quinoxaline derivative **12** inside the active sites of the Bcl-2 (PDB: 4AQ3), EGFR (PDB: 1M17), and VEGFR-2 (PDB: 4ASD) were performed using Molecular Operating Environmental (MOE)[89–92] version 2009.10. All these proteins were downloaded from the protein data bank (**https://www.rcsb.org/**access 14/1/2023). The structure of compound **12** was constructed in 2D using ChemBioDraw. 2014 and exported to MOE. Additionally, the structure of compound **12** was protonated and then the structure was minimized using forcefield MMFF94x, as described previously.[93–96] For Bcl-2 (PDB: 4AQ3), the validation process was carried out by selecting only one chain and deleting all other chains. Moreover, the redocking process was performed, and the co-crystallized ligand (sulfonamide molecule) exhibited binding energy $S = -23.39$ kcal mol^{-1} with RMSD = 1.49 Å, where the alpha triangle placement and London dG as rescoring functions were selected. For EGFR (PDB: 1M17), the validation process reported that the erlotinib (co-crystallized ligand) showed binding energy $S = -17.84$ kcal mol^{-1} with RMSD = 1.73 Å, where the triangle matcher placement and London dG as rescoring functions were selected. Moreover, For VEGFR-2 (PDB: 4ASD), the redocking process of co-crystallized ligand (sorafenib) showed binding energy $S = -16.169$ kcal mol^{-1} with RMSD = 1.484 Å through four hydrogen bonds, where the triangle matcher placement and London dG as rescoring functions were selected.

Abbreviations

BCSCs	Breast cancer stem cells
ROS	Reactive oxygen species
VEGF	Vascular endothelial growth factor
FAD	Food and Drug Administration
EGFR	Epidermal growth factor receptor
TKI	Tyrosine kinase inhibitor
NSCLC	Non-small-cell lung cancer
IC_{50}	Half-maximal inhibitory concentration
MTT	3-(4,5-dimethylthiazol-2-yl)-2,5-diphenyl-2*H*-tetrazolium bromide
Bcl-2	B-cell lymphoma 2
BAX gene	Bcl-2 associated X-protein
p53	Tumor protein P53 or cellular tumor antigen p53
RT-PCR	Real-time reverse transcription–polymerase chain reaction
ADME	Absorption, distribution, metabolism, and excretion
TPSA	Topological polar surface area
PAINS	Pan-assay interference compounds
BBB	Blood–brain barrier
GI	Gastrointestinal
P-gp	Permeability glycoprotein
HSE	Heat shock factor response element
MMP	Mitochondrial membrane potential
PDB	Protein Data Bank

Data availability

All data that support the finding of this study are available in the ESI† data of this article.

Conflicts of interest

The authors declare no conflicts of interest.

References

1 Y. Sun, Y. Liu, X. Ma and H. Hu, *Int. J. Mol. Sci.*, 2021, **22**, 6923.
2 M. M. Rahman, M. R. Islam, S. Akash, M. Harun-Or-Rashid, T. K. Ray, M. S. Rahaman, M. Islam, F. Anika, M. K. Hosain, F. I. Aovi, H. A. Hemeg, A. Rauf and P. Wilairatana, *Biomed. Pharmacother.*, 2022, **153**, 113305.
3 M. M. Rahman, M. R. Islam, S. Akash, S. Shohag, L. Ahmed, F. A. Supti, A. Rauf, A. S. M. Aljohani, W. Al Abdulmonem, A. A. Khalil, R. Sharma and M. Thiruvengadam, *Chem.-Biol. Interact.*, 2022, **368**, 110198.
4 G. L. Wong, S. G. Manore, D. L. Doheny and H.-W. Lo, *Semin. Cancer Biol.*, 2022, **86**, 84–106.
5 R. L. Siegel, K. D. Miller, H. E. Fuchs, A. Jemal and C. A. Cancer, *J. Clin.*, 2022, **72**, 7–33.
6 Q. Wu, J. Li, S. Zhu, J. Wu, C. Chen, Q. Liu, W. Wei, Y. Zhang and S. Sun, *Oncotarget*, 2017, **8**, 27990–27996.
7 M. T. Chen, H. F. Sun, Y. Zhao, W. Y. Fu, L. P. Yang, S. P. Gao, L. D. Li, H. L. Jiang and W. Jin, *Sci. Rep.*, 2017, **7**, 1–8.
8 M. Al-Hajj, M. S. Wicha, A. Benito-Hernandez, S. J. Morrison and M. F. Clarke, *Proc. Natl. Acad. Sci. U. S. A.*, 2003, **100**, 3983–3988.
9 E. Batlle and H. Clevers, *Nat. Med.*, 2017, **23**, 1124–1134.
10 A. F. Karamysheva, *Biochem*, 2008, **73**, 751–762.
11 X. Yuan, Q. Yang, T. Liu, K. Li, Y. Liu, C. Zhu, Z. Zhang, L. Li, C. Zhang, M. Xie, J. Lin, J. Zhang and Y. Jin, *Eur. J. Med. Chem.*, 2019, **179**, 147–165.
12 L. Hlatky, C. Tsionou, P. Hahnfeldt and C. N. Coleman, *Cancer Res.*, 1994, **54**, 6083–6086.
13 N. M. Saleh, M. S. A. El-Gaby, K. El-Adl and N. E. A. Abd El-Sattar, *Bioorg. Chem.*, 2020, **104**, 104350.
14 Y. Huang, X. Chen, M. M. Dikov, S. V Novitskiy, C. A. Mosse, L. Yang and D. P. Carbone, *Blood*, 2007, **110**, 624–631.
15 C. Fontanella, E. Ongaro, S. Bolzonello, M. Guardascione, G. Fasola and G. Aprile, *Ann. Transl. Med.*, 2014, **2**(12), 123–133.
16 P. Wu, T. E. Nielsen and M. H. Clausen, *Trends Pharmacol. Sci.*, 2015, **36**, 422–439.
17 J. Y. Hsu and H. A. Wakelee, *BioDrugs*, 2009, **23**, 289–304.

18 F. Zuccotto, E. Ardini, E. Casale and M. Angiolini, *J. Med. Chem.*, 2010, **53**, 2681–2694.
19 J. Blanc, R. Geney and C. Menet, *Anti-Cancer Agents Med. Chem.*, 2013, **13**, 731–747.
20 Y. Liu and N. S. Gray, *Nat. Chem. Biol.*, 2006, **2**, 358–364.
21 A. M. Srour, D. H. Dawood, E. S. Nossier, R. A. El-Shiekh, A. E. Mahmoud, A. G. Hussien, M. M. Omran and M. M. Ali, *J. Mol. Struct.*, 2023, **1271**, 134130.
22 A. R. Y. A. Ammar, A. M. Sh El-Sharief, A. Belal, S. Y. Abbas, Y. A. Mohamed and A. B. M. Mehany, *Eur. J. Med. Chem.*, 2018, **156**, 918–932.
23 L. Wang, X. Ding, K. Wang, R. Sun, M. Li, F. Wang and Y. Xu, *J. Mol. Struct.*, 2023, **1274**, 134499.
24 J. G. Paez, P. A. Jänne, J. C. Lee, S. Tracy, H. Greulich, S. Gabriel, P. Herman, F. J. Kaye, N. Lindeman, T. J. Boggon, K. Naoki, H. Sasaki, Y. Fujii, M. J. Eck, W. R. Sellers, B. E. Johnson and M. Meyerson, *Science*, 2004, **304**, 1497–1500.
25 R. Montanari, D. Capelli, K. Yamamoto, H. Awaishima, K. Nishikata, A. Barendregt, A. J. R. Heck, F. Loiodice, F. Altieri, A. Paiardini, A. Grottesi, L. Pirone, E. Pedone, F. Peiretti, J. M. Brunel, T. Itoh and G. Pochetti, *J. Med. Chem.*, 2020, **63**, 4811–4823.
26 W. Zhou, D. Ercan, L. Chen, C.-H. Yun, D. Li, M. Capelletti, A. B. Cortot, L. Chirieac, R. E. Iacob, R. Padera, J. R. Engen, K.-K. Wong, M. J. Eck, N. S. Gray and P. A. Jänne, *Nature*, 2009, **462**, 1070–1074.
27 H. A. Yu, M. E. Arcila, N. Rekhtman, C. S. Sima, M. F. Zakowski, W. Pao, M. G. Kris, V. A. Miller, M. Ladanyi and G. J. Riely, *Clin. Cancer Res.*, 2013, **19**, 2240–2247.
28 S. S. Ramalingam, J. Vansteenkiste, D. Planchard, B. C. Cho, J. E. Gray, Y. Ohe, C. Zhou, T. Reungwetwattana, Y. Cheng, B. Chewaskulyong, R. Shah, M. Cobo, K. H. Lee, P. Cheema, M. Tiseo, T. John, M.-C. Lin, F. Imamura, T. Kurata, A. Todd, R. Hodge, M. Saggese, Y. Rukazenkov and J.-C. Soria, *N. Engl. J. Med.*, 2020, **382**, 41–50.
29 C.-C. Lan, P.-C. Hsieh, C.-Y. Huang, M.-C. Yang, W.-L. Su, C.-W. Wu and Y.-K. Wu, *World J. Clin. Cases*, 2022, **10**, 6360–6369.
30 R. T. Dungo and G. M. Keating, *Drugs*, 2013, **73**, 1503–1515.
31 N. M. Jackson and B. P. Ceresa, *Exp. Cell Res.*, 2017, **356**, 93–103.
32 P. Shi, S. Zhang, L. Zhu, G. Qian, H. Ren, S. S. Ramalingam, M. Chen and S.-Y. Sun, *Transl. Oncol.*, 2019, **12**, 705–713.
33 M. M. S. Wassel, Y. A. Ammar, G. A. M. Elhag Ali, A. Belal, A. B. M. Mehany and A. Ragab, *Bioorg. Chem.*, 2021, **110**, 104794.
34 A. Furlan, F. Colombo, A. Kover, N. Issaly, C. Tintori, L. Angeli, V. Leroux, S. Letard, M. Amat, Y. Asses, B. Maigret, P. Dubreuil, M. Botta, R. Dono, J. Bosch, O. Piccolo, D. Passarella and F. Maina, *Eur. J. Med. Chem.*, 2012, **47**, 239–254.
35 F. Colombo, C. Tintori, A. Furlan, S. Borrelli, M. S. Christodoulou, R. Dono, F. Maina, M. Botta, M. Amat, J. Bosch and D. Passarella, *Bioorg. Med. Chem. Lett.*, 2012, **22**, 4693–4696.
36 A. Ragab, D. M. Elsisi, O. A. Abu Ali, M. S. Abusaif, A. A. Askar, A. A. Farag and Y. A. Ammar, *Arabian J. Chem.*, 2022, **15**, 103497.
37 E. A. Fayed, Y. A. Ammar, M. A. Saleh, A. H. Bayoumi, A. Belal, A. B. M. Mehany and A. Ragab, *J. Mol. Struct.*, 2021, **1236**, 130317.
38 A. Burguete, E. Pontiki, D. Hadjipavlou-Litina, R. Villar, E. Vicente, B. Solano, S. Ancizu, S. Pérez-Silanes, I. Aldana and A. Monge, *Bioorg. Med. Chem. Lett.*, 2007, **17**, 6439–6443.
39 R. Ingle, R. Marathe, D. Magar, H. M. Patel and S. J. Surana, *Eur. J. Med. Chem.*, 2013, **65**, 168–186.
40 D. M. Elsisi, A. Ragab, A. A. Elhenawy, A. A. Farag, A. M. Ali and Y. A. Ammar, *J. Mol. Struct.*, 2022, **1247**, 131314.
41 X. Jiang, K. Wu, R. Bai, P. Zhang and Y. Zhang, *Eur. J. Med. Chem.*, 2022, **229**, 114085.
42 E. A. Fayed, Y. A. Ammar, A. Ragab, N. A. Gohar, A. B. M. Mehany and A. M. Farrag, *Bioorg. Chem.*, 2020, **100**, 103951.
43 A. Levitzki, *Acc. Chem. Res.*, 2003, **36**, 462–469.
44 Z. H. Chohan, A. U. Shaikh and C. T. Supuran, *J. Enzyme Inhib. Med. Chem.*, 2006, **21**, 733–740.
45 S. T. Bhaskaran and P. Mathew, *J. Mol. Struct.*, 2022, **1251**, 132071.
46 T. Rescigno, M. F. Tecce and A. Capasso, *Open Biochem. J.*, 2018, **12**, 46–64.
47 V. Kartsev, K. S. Shikhaliev, A. Geronikaki, S. M. Medvedeva, I. V Ledenyova, M. Y. Krysin, A. Petrou, A. Ciric, J. Glamoclija and M. Sokovic, *Eur. J. Med. Chem.*, 2019, **175**, 201–214.
48 J. L. Segura and N. Martín, *Angew. Chem., Int. Ed.*, 2001, **40**, 1372–1409.
49 A. Bazgir and A. M. Astaraki, *Phosphorus, Sulfur Silicon Relat. Elem.*, 2011, **186**, 1916–1921.
50 A. A. Fadda, A. Fekri and N. M. Bayoumy, *RSC Adv.*, 2015, **5**, 80844–80852.
51 A. A. Fadda, M. A. El Salam, E. H. Tawfik, E. M. Anwar and H. A. Etman, *RSC Adv.*, 2017, **7**, 39773–39785.
52 S. A. Shaker and M. I. Marzouk, *Molecules*, 2016, **21**, 155.
53 X. C. Liu, D. Lai, Q. Z. Liu, L. Zhou, Q. Liu and Z. L. Liu, *Molecules*, 2016, **21**, 1665.
54 E. Vitaku, D. T. Smith and J. T. Njardarson, *J. Med. Chem.*, 2014, **57**, 10257–10274.
55 R. S. Kumar, A. I. Almansour, N. Arumugam, D. M. Q. Althomili, M. Altaf, A. Basiri, D. Kotresha, T. Sai Manohar and S. Venketesh, *Bioorg. Chem.*, 2018, **77**, 263–268.
56 B. Li, E. D. Jones, E. Zhou, L. Chen, D. C. Baylis, S. Yu, M. Wang, X. He, J. A. V. Coates, D. I. Rhodes, G. Pei, J. J. Deadman, X. Xie and D. Ma, *Bioorg. Med. Chem. Lett.*, 2010, **20**, 5334–5336.
57 M. M. Abdelgalil, Y. A. Ammar, G. A. M. Elhag Ali, A. K. Ali and A. Ragab, *J. Mol. Struct.*, 2023, **1274**, 134443.
58 M. S. Jan, S. Ahmad, F. Hussain, A. Ahmad, F. Mahmood, U. Rashid, O.-R. Abid, F. Ullah, M. Ayaz and A. Sadiq, *Eur. J. Med. Chem.*, 2020, **186**, 111863.
59 P. Devi, A. Bishnoi and V. Singh, *ChemistrySelect*, 2019, **4**, 629–632.

60 Y. Arun, K. Saranraj, C. Balachandran and P. T. Perumal, *Eur. J. Med. Chem.*, 2014, **74**, 50–64.
61 G. Li Petri, M. V. Raimondi, V. Spanò, R. Holl, P. Barraja and A. Montalbano, *Top. Curr. Chem.*, 2021, **379**, 34.
62 C. Bhat and S. G. Tilve, *RSC Adv.*, 2014, **4**, 5405–5452.
63 Z. Guo, Y. Xu, Y. Peng, H. ur Rashid, W. Quan, P. Xie, L. Wu, J. Jiang, L. Wang and X. Liu, *Bioorg. Med. Chem. Lett.*, 2019, **29**, 1133–1137.
64 T. Owa, H. Yoshino, T. Okauchi, K. Yoshimatsu, Y. Ozawa, N. H. Sugi, T. Nagasu, N. Koyanagi and K. Kitoh, *J. Med. Chem.*, 1999, **42**, 3789–3799.
65 C. T. Supuran, *Expert Opin. Invest. Drugs*, 2003, **12**, 283–287.
66 B. Sloan and N. S. Scheinfeld, *Curr. Opin. Invest. Drugs*, 2008, **9**, 1324–1335.
67 J. A. Plumb, P. W. Finn, R. J. Williams, M. J. Bandara, M. R. Romero, C. J. Watkins, N. B. La Thangue and R. Brown, *Mol. Cancer Ther.*, 2003, **2**, 721–728.
68 A. B. Suttle, K. F. Grossmann, D. Ouellet, L. E. Richards-Peterson, G. Aktan, M. S. Gordon, P. M. LoRusso, J. R. Infante, S. Sharma, K. Kendra, M. Patel, S. Pant, H.-T. Arkenau, M. R. Middleton, S. C. Blackman, J. Botbyl and S. W. Carson, *J. Clin. Pharmacol.*, 2015, **55**, 392–400.
69 A. Ragab, M. S. Abusaif, N. A. Gohar, D. S. Aboul-Magd, E. A. Fayed and Y. A. Ammar, *Bioorg. Chem.*, 2023, **131**, 106307.
70 A. S. Hassan, N. M. Morsy, W. M. Aboulthana and A. Ragab, *Drug Dev. Res.*, 2022, **84**, 3–24.
71 R. Ayman, M. S. Abusaif, A. M. Radwan, A. M. Elmetwally and A. Ragab, *Eur. J. Med. Chem.*, 2023, **249**, 115138.
72 Y. A. Ammar, G. A. M. Elhagali, M. S. Abusaif, M. R. Selim, M. A. Zahran, T. Naser, A. B. M. Mehany and E. A. Fayed, *Med. Chem. Res.*, 2021, **30**, 1649–1668.
73 M. S. Abusaif, M. Fathy, M. A. Abu-Saied, A. A. Elhenawy, A. B. Kashyout, M. R. Selim and Y. A. Ammar, *J. Mol. Struct.*, 2021, **1225**, 129297.
74 Y. A. Ammar, A. A. Farag, A. M. Ali, S. A. Hessein, A. A. Askar, E. A. Fayed, D. M. Elsisi and A. Ragab, *Bioorg. Chem.*, 2020, **99**, 103841.
75 Y. A. Ammar, A. A. Farag, A. M. Ali, A. Ragab, A. A. Askar, D. M. Elsisi and A. Belal, *Bioorg. Chem.*, 2020, **104**, 104164.
76 J. Lin, P. Wang, Z. Zhang, G. Xue, D. Zha, J. Wang, X. Xu and Z. Li, *Synth. Commun.*, 2020, **50**, 823–830.
77 J. M. Neri, L. N. Cavalcanti, R. M. Araújo and F. G. Menezes, *Arabian J. Chem.*, 2020, **13**, 721–739.
78 S. A. Ibrahim, A. Ragab and H. A. El-Ghamry, *Appl. Organomet. Chem.*, 2022, **36**, 1–17.
79 M. M. S. Wassel, A. Ragab, G. A. M. Elhag Ali, A. B. M. Mehany and Y. A. Ammar, *J. Mol. Struct.*, 2021, **1223**, 128966.
80 R. Z. Batran, S. M. El-Daly, W. A. El-Kashak and E. Y. Ahmed, *Chem. Biol. Drug Des.*, 2022, **99**, 470–482.
81 M. Eldeeb, E. F. Sanad, A. Ragab, Y. A. Ammar, K. Mahmoud, M. M. Ali and N. M. Hamdy, *Biomedicines*, 2022, **10**, 722.
82 A. Ragab, Y. A. Ammar, A. Ezzat, A. M. Mahmoud, M. Basseem, I. Mohamed, A. S. El-tabl and R. S. Farag, *Comput. Biol. Med.*, 2022, **145**, 105473.
83 A. Y. Alzahrani, Y. A. Ammar, M. Abu-Elghait, M. A. Salem, M. A. Assiri, T. E. Ali and A. Ragab, *Bioorg. Chem.*, 2022, **119**, 105571.
84 R. Ayman, A. M. Radwan, A. M. Elmetwally, Y. A. Ammar and A. Ragab, *Arch. Pharm.*, 2023, **356**, e2200395.
85 K. E. Saadon, N. M. H. Taha, N. A. Mahmoud, G. A. M. Elhagali and A. Ragab, *J. Iran. Chem. Soc.*, 2022, **19**, 3899–3917.
86 A. Ragab, S. A. Fouad, Y. A. Ammar, D. S. Aboul-magd and M. S. Abusaif, *Antibiotics*, 2023, **12**, 128.
87 E. A. Fayed, M. Mohsen, S. M. A. El-Gilil, D. S. Aboul-Magd and A. Ragab, *J. Mol. Struct.*, 2022, **1262**, 133028.
88 A. E. Azab, M. S. Alesawy, W. M. Eldehna, A. Elwan and I. H. Eissa, *Arch. Pharm.*, 2022, **355**, 2200133.
89 E. S. A. E. H. Khattab, A. Ragab, M. A. Abol-Ftouh and A. A. Elhenawy, *J. Biomol. Struct. Dyn.*, 2021, **40**, 13291–13309.
90 S. A. El-Kalyoubi, A. Ragab, O. A. Abu Ali, Y. A. Ammar, M. G. Seadawy, A. Ahmed and E. A. Fayed, *Pharmaceuticals*, 2022, **15**, 376.
91 H. F. Rizk, M. A. El-Borai, A. Ragab, S. A. Ibrahim and M. E. Sadek, *Polycyclic Aromat. Compd.*, 2023, **43**, 500–522.
92 A. S. Hassan, N. M. Morsy, W. M. Aboulthana and A. Ragab, *RSC Adv.*, 2023, **13**, 9281–9303.
93 A. Ezzat, M. B. I. Mohamed, A. M. Mahmoud, R. S. Farag, A. S. El-Tabl and A. Ragab, *J. Mol. Struct.*, 2022, **1251**, 132004.
94 A. Y. Alzahrani, Y. A. Ammar, M. A. Salem, M. Abu-Elghait and A. Ragab, *Arch. Pharm.*, 2022, **355**, e2100266.
95 H. Ali Mohamed, Y. A. Ammar, G. A. m. Elhagali, H. A. Eyada, D. S. Aboul-Magd and A. Ragab, *ACS Omega*, 2022, **7**, 4970–4990.
96 R. R. Raslan, Y. A. Ammar, S. A. Fouad, S. A. Hessein, N. A. M. Shmiess and A. Ragab, *RSC Adv.*, 2023, **13**, 10440–10458.